Gravity wave drag parameterizations for Earth's atmosphere

Christopher G Kruse[1], Jadwiga H Richter[2], M. Joan Alexander[1], Julio T Bacmeister[2], Christopher Heale[3], and Junhong Wei[4]

[1]NorthWest Research Associates, Boulder, CO, USA
[2]Climate and Global Dynamics Laboratory, National Center for Atmospheric Research, Boulder, CO, USA
[3]Department of Physical Sciences, Embry–Riddle Aeronautical University, Daytona Beach, Florida, USA
[4]School of Atmospheric Sciences and Guangdong Province Key Laboratory for Climate Change and Natural Disaster Studies, Sun Yat-sen University, and Southern Marine Science and Engineering Guangdong Laboratory (Zhuhai), Zhuhai, China

January 17, 2023

Abstract

Atmospheric gravity waves (GWs), or buoyancy waves, transport momentum and energy through Earth's atmosphere. GWs are important at nearly all levels of the atmosphere, though, the momentum they transport is particularly important in general circulation of the middle and upper atmosphere. Primary sources of atmospheric GWs are flow over mountains, moist convection, and imbalances in jet/frontal systems. Secondary GWs can also be generated as a result of dissipation of a primary GWs. Gravity waves typically have horizontal wavelengths of 10's to 100's of kilometers, though, they can have scales of 1's to 1000's of kilometers as well. Current effective resolutions of climate models, and even numerical weather prediction models, do not resolve significant portions of the momentum- and energy-flux-carrying GW spectrum, and so parameterizations are necessary to represent under- and unresolved GWs in most current models. Here, an overview of GWs generated by orography, convection, jet/front systems, primary wave breaking, and secondary wave generation is provided. The basic theory of GW generation, propagation, and dissipation relevant to parameterization is presented. Conventionally used GW parameterizations are then reviewed. Lastly, we describe uncertainties and parameter tuning in current parameterizations and discuss known processes that are currently missing.

Gravity wave drag parameterizations for Earth's atmosphere

Christopher G. Kruse[1], Jadwiga H. Richter[2], M. Joan Alexander[1], Julio T. Bacmeister[2], Christopher Heale[3], Junhong Wei[4]

[1]NorthWest Research Associates, Boulder, CO, USA
[2]Climate and Global Dynamics Laboratory, National Center for Atmospheric Research, Boulder, CO, USA
[3]Department of Physical Sciences, Embry–Riddle Aeronautical University, Daytona Beach, Florida, USA
[4]School of Atmospheric Sciences and Guangdong Province Key Laboratory for Climate Change and Natural Disaster Studies, Sun Yat-sen University, and Southern Marine Science and Engineering Guangdong Laboratory (Zhuhai), Zhuhai, China

Chapter 11 of AGU Book entitled:
"Fast Physics in Large Scale Atmospheric Models: Parameterization, Evaluation, and Observations",
Editors: Yangang Liu; Pavlos Kollias; Leo Donner (advisor)

Corresponding Author:
Christopher G. Kruse, ckruse@nwra.com

Abstract

Atmospheric gravity waves (GWs), or buoyancy waves, transport momentum and energy through Earth's atmosphere. GWs are important at nearly all levels of the atmosphere, though, the momentum they transport is particularly important in general circulation of the middle and upper atmosphere. Primary sources of atmospheric GWs are flow over mountains, moist convection, and imbalances in jet/frontal systems. Secondary GWs can also be generated as a result of dissipation of a primary GWs. Gravity waves typically have horizontal wavelengths of 10's to 100's of kilometers, though, they can have scales of 1's to 1000's of kilometers as well. Current effective resolutions of climate models, and even numerical weather prediction models, do not resolve significant portions of the momentum- and energy-flux-carrying GW spectrum, and so parameterizations are necessary to represent under- and unresolved GWs in most current models. Here, an overview of GWs generated by orography, convection, jet/front systems, primary wave breaking, and secondary wave generation is provided. The basic theory of GW generation, propagation, and dissipation relevant to parameterization is presented. Conventionally used GW parameterizations are then reviewed. Lastly, we describe uncertainties and parameter tuning in current parameterizations and discuss known processes that are currently missing.

11.1 Introduction and basic equations

Gravity waves (GWs), or buoyancy waves, are waves in Earth's atmosphere for which buoyancy is the restoring force. Most are familiar with the concentric waves that form on the surface of the water and emanate away from the perturbation from a falling stone: such waves exist on the boundary of a denser fluid (water) and less dense air above. Atmospheric GWs are analogous to surface waves, with the same buoyancy restoring force. However, the atmosphere is continuously stratified, with a more-or-less smooth decrease in potential density with height. In the continuously stratified atmosphere, lower-level atmospheric GW perturbations displace the stably-stratified atmospheric flows above, allowing propagation in the vertical as well as the horizontal (i.e. in all three dimensions).

Sources of atmospheric GWs are numerous. Essentially any process, often an instability, that produces transient perturbations of air parcels (e.g. in their altitude or potential density) can be a GW source. However, three primary sources are flow over mountains, moist convection, and imbalances associated with jets and fronts. Recent studies have focused on secondary GWs generated as a result of localized breaking/dissipation of a primary GW. Gravity waves typically have horizontal wavelengths of 10's to 100's of kilometers, and vertical scales of 3 to 30 km, with periods ranging from about 10 min to several hours. Still, GWs, often orographically forced, with horizontal scales of a few kilometers are not uncommon. Some sources (e.g. jet/front imbalances) can generate waves with larger horizontal wavelengths, too, with scales of ≈500 km and periods between 6 and 24 hours. These waves are typically classified as inertia-gravity waves, where the Coriolis effect cannot be neglected. The properties of GWs at various levels of the atmosphere vary dependent on the GW source, altitude, and atmospheric properties that they have propagated through.

Numerous review articles (e.g. Smith 1979, Fritts and Alexander 2003, Teixiera 2014) and textbooks (e.g. Holton 2004) present the basic, and not so basic, theory of atmospheric GWs. For full derivations and rigorous mathematical treatment, the reader is directed to these references. Here, basic relations from linear GW theory are presented to demonstrate fundamental ideas relevant to GW parameterizations.

Characteristics of GWs are governed by a dispersion relation that gives the relationship between the wave frequency and its horizontal and vertical wavenumbers. The following dispersion relation for two-dimensional (i.e. x and z) gravity waves in a non-rotating atmosphere can be derived from linearized Boussinesq equations of motions (e.g. Holton et al. 2004):

$$\omega^{*2} = (\omega - Uk)^2 = \frac{N^2 k^2}{(k^2+m^2)}. \qquad (1)$$

Here, ω^{*2} is the intrinsic frequency of the wave, which is the oscillation frequency an air parcel experiences as it is advected through the wave, ω is the wave, or parcel oscillation, frequency relative to the ground, $k = 2\pi/\lambda_x$ and $m = 2\pi/\lambda_z$ are the horizontal and vertical wavenumbers, respectively, U is the background wind, and $N^2 = \frac{g}{\theta}\frac{\partial\theta}{\partial z}$ is the background atmospheric buoyancy frequency where θ is the background potential temperature.

(1) can be solved for the vertical wavenumber as follows:

$$m^2 = \frac{k^2(N^2-\omega^{*2})}{\omega^{*2}} \qquad (2)$$

Another key property of gravity waves is the horizontal wave phase speed, c_{px}:

$$c_{px} = \frac{\omega}{k} \qquad (3)$$

The above is the wave phase speed relative to the ground. The intrinsic wave phase speed, or phase speed relative to the mean wind is defined as:

$$c_{px}^* = \frac{\omega^*}{k} = c_{px} - U = \pm \frac{N}{(k^2+m^2)^{\frac{1}{2}}} \qquad (4)$$

The wave phase speed, as will be described in later sections, largely determines whether waves are able to propagate upwards and where they will break and deposit momentum to the mean flow. Horizontal group velocity, c_{gx}, or the speed of energy propagation, is related to the intrinsic phase speed through:

$$c_{gx} = \frac{\partial\omega}{\partial k} = U + c_{gx}^* \qquad (5)$$

where

$$c_{gx}^* = \frac{\partial\omega^*}{\partial k} = c_{px}^*\left(1 - \frac{k^2}{k^2+m^2}\right). \qquad (6)$$

For stationary orographic GWs (OGWs), or mountain waves (MWs), the ground-relative phase speed is zero, so the horizontal intrinsic phase speed exactly opposes the background wind (i.e. $c_{px}^* = -U$ via (4)). In the hydrostatic limit ($k \ll m$), the horizontal group velocity is the same as the horizontal phase speed. This means the horizontal group velocity is zero for hydrostatic OGWs, therefore these OGWs primarily stay over the orography that generated them. However, for $k \sim m$, the horizontal group velocity becomes non-zero in the direction of the background flow for non-hydrostatic OGWs, leading to their energy propagation and presence downstream. The speed at which the GW energy propagates in the vertical is described by the vertical group velocity:

$$c_{gz} = \frac{\partial\omega}{\partial m} = \frac{\omega^*}{m}\left(\frac{m^2}{m^2+k^2}\right) \qquad (7)$$

In the hydrostatic limit and using (1) and (3), the vertical group velocity becomes

$$c_{gz} \approx \pm\frac{(c_{px}-U)^2 k}{N}. \qquad (8)$$

According to (8), the speed at which hydrostatic GWs propagate upward is proportional to the squared intrinsic phase speed and inversely proportional to horizontal wavelength and stability. For a given environment, GWs with shorter horizontal scales propagate upward more quickly, at least until non-hydrostatic effects become important (i.e. when k becomes comparable to m).

11.1.2 Mountain Waves

MWs are GWs generated by stably-stratified flow over mountains. MWs are perhaps the most well-known type of atmospheric GWs, being quite visible, quasi-stationary, and the subject of research for at least a century (e.g. Lyra 1940, Smith 2019). MWs typically form above and downwind of topographic features. Their presence is often indicated by quasi-stationary lenticular clouds visible from the ground and in satellite images. The properties of mountain waves are determined by the size and shape of the topography as well as by the vertical profiles of wind, temperature, and moisture in the surrounding flow. Linear theory can predict the general features of MWs when the mountain height is small in comparison to the vertical wavelength of the wave.

Conventional linear MW theory assumes MWs are stationary, with zero ground-relative horizontal phase speed or frequency ($c_{px}, \omega = 0$). Such MWs have phase lines (e.g. wave crests) that tilt upstream with height. The dispersion relation, (2), can be written for stationary waves as:

$$m^2 = k^2 \left(\frac{N^2-(Uk)^2}{(Uk)^2}\right). \qquad (9)$$

Solutions of flow over small-scale, sinusoidal ridges, where the intrinsic frequency of these parcels is higher than the buoyancy frequency (i.e. $Uk > N$ and hence m in (9) is imaginary), decay exponentially with height. Flow over wider ridges (for which $f < Uk < N$) generate MWs that propagate vertically (Smith 1979, Durran 1986b, Holton 1992).

Linear theory has also been used successfully to describe the basic properties of mountain waves generated by compact, or spatially limited, obstacles (e.g.: Lyra 1940,1943, Queney 1947, Scorer 1949, Smith 1979, Durran 2003). Some non-linear solutions to flow over compact obstacles exist as well (e.g. Huppert and Miles 1969), though, here linear theory is the focus. Flow over an isolated ridge will generate a horizontal spectrum of waves, and each wave component will either propagate upwards or decay depending on its m derived from (9) for its k. (6) shows that for a 2D flow over a wider ridge, the (hydrostatic) horizontal group velocity is close to the horizontal phase speed so wave energy is contained above the mountain only, with little propagation downstream of the mountain. However, if the mountain ridge is sufficiently narrow, nonhydrostatic waves with downstream group velocity can be generated. If atmospheric conditions are such that $m^2 > 0$ near the surface, but becomes negative further aloft, MWs are reflected and a train of trapped lee waves may be generated downstream of the forcing (Scorer 1949). This can happen, for example, when there is strong positive vertical shear of the wind, $U_z > 0$, or a sharp reduction in N due to an inversion, over narrow ridges. In three dimensional flows over obstacles with finite scales in both horizontal dimensions, oblique modes (those at an angle between 0° and 90° to the incident wind) can also propagate downstream, even in the hydrostatic limit (Smith 1980, Sato et al. 2012, Jiang et al. 2019). This contributes to the appearance of broad, large-amplitude perturbations often seen in satellite data significantly downwind of large orographic features such as the Antarctic Peninsula and the terminus of the Andes (e.g. Alexander et al. 2009, Hoffmann et al. 2013, Hoffmann et al. 2016). High-resolution, three-dimensional simulations have been critical in developing realistic representations of MW generation and have shown that three-dimensional dispersion spreads the gravity wave energy, reducing the amplitude with increasing height relative to only vertically-propagating MWs (Eckermann et al 2015).

In addition to upward propagating mountain waves, flow in a mountainous region can produce low-level blocking upstream and downslope windstorms downstream. Low-level blocking occurs when the mean flow does not have enough kinetic energy to traverse an obstacle and either stops upstream or diverges around the obstacle (Pierrehumbert and Wyman, 1985, Lin and Wang 1985, Smolarkiewicz and Rotunno 1990, Hughes et al. 2009). Blocking can significantly impact the waves generated, the orographic drag on the flow, and precipitation patterns. The Froude number, $F_r = \frac{U}{Nh_m}$ where h_m is the height of the mountain, in large part determines whether blocking will occur (Pierrehumbert and Wyman, 1985, Lin and Wang 1996). When $F_r >> 1$, the flow is said to be linear. A flow in this regime has enough kinetic energy to easily traverse the mountain and dynamic wave amplitudes are small (i.e. $u' << U$). When $F_r \sim 1$, the validity of linear theory is questionable and nonlinear terms become important. When $F_r < 1$, the flow is strongly nonlinear and low-level flow may not traverse the mountain, becoming blocked upstream or diverting around the obstacles (Shepherd 1956, Drazin 1961, Leo et al. 2016). The evolution of nonlinear low-level flows depends on obstacle aspect ratios (e.g. Miranda and James 1992; Olafsson and Bougeault 1996), orientation, and shape (Phillips 1984). In this situation, the pressure force by the atmosphere on the orography, and the corresponding drag by the orography back on the low-level flow in part due to the non-linear blocked flow and in part due to a vertically-propagating MW response in the atmosphere a bit further aloft. When orographic blocking occurs, the momentum flux of the vertically-propagating MWs is reduced relative to what linear theory alone predicts.

Downslope wind storms can exist on a downstream side of a mountain, in particular ones with steep leeside slopes, with wind gusts that can exceed 50 m s^{-1} (Clark and Peltier 1977, Lilly 1978, Lilly and Klemp 1979, Peltier and Clark 1979, Smith 1985, Bacmeister and Pierrehumbert 1988, Durran 1990, Durran 1986a). In addition, flow configurations analogous to hydraulic trans-critical flows (Smith 1985, Durran 1986a) can form leading to significantly enhanced drag on the low-level flow. These flows are responsible for many of the named downslope winds that occur around large mountain ranges: e.g. Chinooks, Santa Anas, Föhns, Zondas. Nonlinear two-dimensional flow over obstacles has been investigated extensively over several decades (e.g.: Clark and Peltier 1977, Durran and Klemp 1983, Clark and Peltier 1984, Durran and Klemp 1983, Durran 1986a, Durran and Klemp 1987, Bacmeister and Schoeberl 1989, Lott 1998, Farmer and Armi 1999, Winters and Armi 2014). These studies have led to important insights about stability, hydraulic analogs, downslope winds, and time-dependence in mountain wave flows. Results from 3D numerical simulations were used explicitly in developing more complete orographic gravity wave drag parameterization schemes for global models (e.g. Lott and Miller 1997, Scinocca and McFarlane 2000, Webster et al. 2003).

In addition to drag from mesoscale OGWs, another important source of low-level orographic drag in the atmosphere is turbulent orographic form drag (TOFD). This is drag produced in the boundary layer by small obstacles (< 5 km). In contrast to OGW, this drag is produced in all stratification-regimes, but does not carry momentum flux out of the boundary layer (e.g. Beljaars et al 2003).

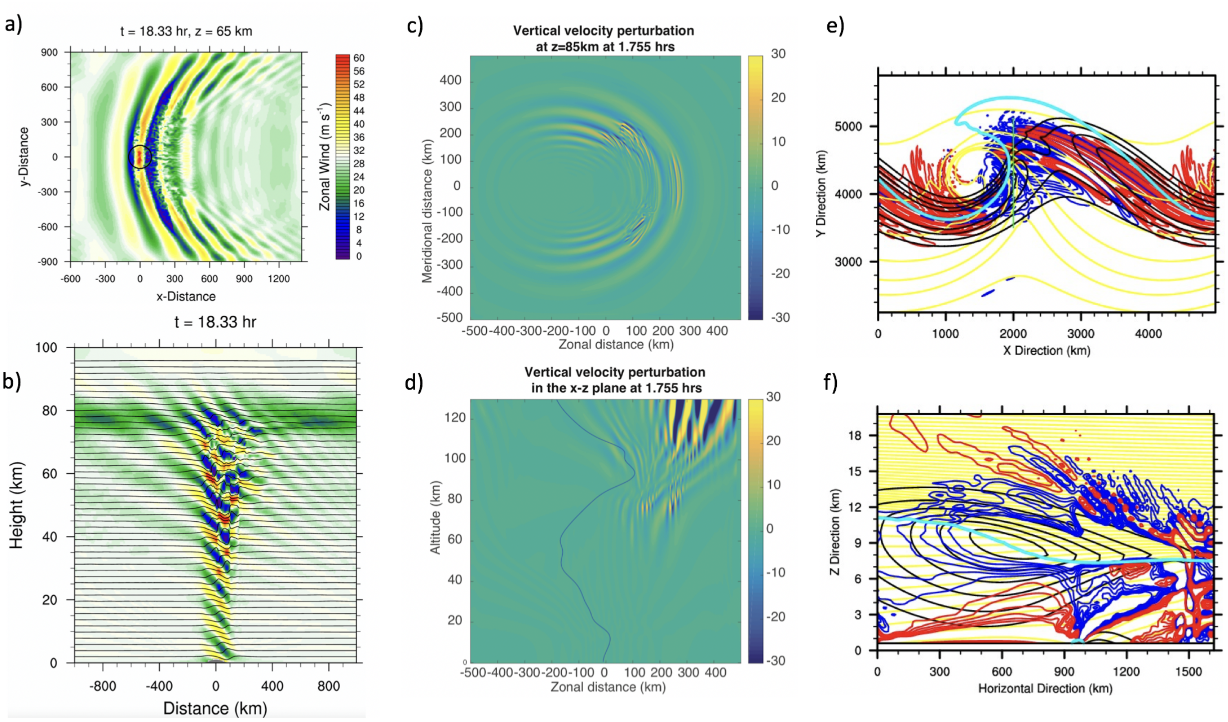

Figure 1: Depiction of three dominant sources of GWs: a, b) Orographic, c, d) Convective, and e, f) Frontal. Corresponding animations can be found at: http://www.cgd.ucar.edu/staff/jrichter/animations.html

a, b): 3D simulation of orographic gravity waves by an 200-km-wide, 1000-m-high isotropic compact-cosine mountain using the WRF model. (bottom) Zonal winds (color shaded) and isentropes (contoured) are shown in the x-z slice through the middle of the 3-D domain. (top) Zonal winds (color shaded) are shown in an x-y slice through z = 65 km. The single contour shows the spatial extent of the mountain. Both panels are from 18.33 hours after the start of cross-mountain flow, just after wave breaking has begun. Buoyancy frequency, N, is 0.02 s^{-1} and constant environmental zonal mean wind of 30 m s^{-1} was specified. A Rayleigh damping layer starts at z = 70 km. The WRF setup here is a 3-D extension of that described by Kruse and Smith (2018).

c, d): 3D simulation of convectively generated gravity waves using the Complex Geometry Compressible Atmospheric Model (CGCAM) (Felton and Lund, 2006). Latent heating is used as a proxy for convection. Top panel shows a cross-section at z=85 km 1.755 hrs into the simulation, whereas the bottom panel shows a vertical cross-section through the center of the domain at the same time. Shading indicates vertical velocity perturbations. Solid thin line depicts the background zonal mean wind profile. Adapted from Heale et al. 2020.

e, f) Gravity waves simulated by a high-resolution idealized weak moist baroclinic wave simulation using the WRF model in Wei and Zhang (2014): (e) The horizontal view of the simulated 1-km temperature (yellow lines; contour interval is 5 K), 7-km dynamic tropopause where potential vorticity equals 1.5 PVU (turquoise lines), 8-km horizontal wind (black lines; contours at 40, 45, 50, and 55 m s^{-1}*), and 12-km horizontal divergence (blue lines, positive; red lines, negative; contour interval is* $2.0*10^{-6}$ s^{-1}*; range is between* $-1.2*10^{-5}$ s^{-1} *and* $1.2*10^{-5}$ s^{-1}*; zero value omitted). (f) The vertical cross section along the green line in (e) for the simulated potential temperature (yellow lines; contour interval is 5 K), dynamic tropopause where potential vorticity equals 1.5 PVU (turquoise lines), horizontal wind (black lines; contours at 30, 35, 40, 45, 50, 55, 60 and 65 m* s^{-1}*), and horizontal divergence (blue lines, positive; red lines, negative; contour interval is* $2.0*10^{-6}$ s^{-1}*; range is between* $-1.2*10^{-5}$ s^{-1} *and* $1.2*10^{-5}$ s^{-1}*; zero value omitted). Figure courtesy of J. Wei.*

Figures 1a, b show the vertical and horizontal properties of mountain waves generated over an isolated obstacle. In this case, the MWs forced by the topography are linear and approximately hydrostatic. These hydrostatic waves primarily stay over the idealized mountain below (Fig. 1b). Wave amplitudes grow with height, resulting in breaking in the upper atmosphere above $z \sim 60$ km. Figure 1a shows MW perturbations in the horizontal plane at the height of 65 km. Strongest perturbations are right over the obstacle and show a bow-shaped structure with decaying amplitudes away from the obstacle in the direction perpendicular to the mean flow. At 65 km in this particular simulation, gravity wave breaking has already begun.

The supplementary Animation 1 (http://www.cgd.ucar.edu/staff/jrichter/animations.html) shows the time evolution of MW generation shown in Figures 1a,b. Gravity waves form almost immediately over the obstacle and then propagate upwards. Smaller-scale MWs appear first, within ~ 5 hours, at mesospheric altitudes, consistent with (8). The MW at $z = 65$ km grows in amplitude and scale with time, as longer waves build in having had enough time to reach this altitude. By ~15 hours into the simulation, the MW field begins to break, in this case via wave overturning and static instability as no turbulence parameterization was used. The entire wave field quickly dissipates after ~ 24 hrs into the simulation, in part due to wave breaking and also in part due cessation of cross-barrier flow at $t = 24$ hrs. The complexity of the wave breaking is well visualized by the right-hand panel of supplementary Animation 1 which shows a horizontal cross-section through the wind field at 65 km. Up to 15 hrs into the visualization, coherent wave crest/troughs are present throughout the model domain. After breaking begins, turbulent features at the grid-scale become apparent and secondary waves are generated, which appear throughout the doubly-periodic domain. Supplementary Animation 2 shows the characteristics of the gravity wave field at various altitudes at 18.33 hours into the simulation. The visualization shows largest wave amplitudes within 200 km from the center of the obstacle in the cross-wind direction, with waves extending in a quasi V-shape away from the obstacle, if looking in the direction of the mean wind at the wave field. Hence, most of the perturbations associated with the flow over the obstacle are directly over the obstacle and in the bow-shaped region downwind and away from the obstacle. Wave breaking begins at 47 km in this particular simulation, intensifying with altitude.

11.1.3 Convectively generated gravity waves

Moist convection is another prominent source of GWs and the dominant GW source in the Tropics. Two and three-dimensional numerical simulations of convection reveal that convection excites a broad spectrum of waves with horizontal wavelengths between 10 and 100's km, and periods from a few minutes to several hours (e.g.: Alexander et al. 1995, Alexander and Holton 1997, Piani et al. 2000, Piani and Durran 2001). The vertical wavelengths of convectively generated gravity waves can vary between several kilometers up to 40 km (e.g. Alexander and Holton 2004). Convectively generated gravity waves are rarely symmetric in the horizontal plane, and typically have a preferred propagation direction, which is determined by the vertical structure of the horizontal wind within which the convection and GW generation occur (Beres et al. 2002).

Generation of gravity waves by convection is a complex nonlinear process, but has been described via three linear mechanisms, all of which are ultimately a response to latent heating:

1) Thermal or diabatic forcing: in this mechanism temporal and spatial variations of convective heating produce perturbations in potential density that force a spectrum of GWs. This mechanism was found to be of primary importance by Bretherton et al 1988, Lin et al. 1998, Chun and Baik 1998, and Pandya and Alexander (1999). Based on 2-D linearized governing equations, the dominant characteristics of the spectrum of convectively generated GWs the generated by thermal forcing are determined by the vertical scale of the heating region and the horizontal wavenumber and frequency distribution of the heating (Holton et al. 2002). Beres (2004) has shown that the three-dimensional wave forcing problem can be treated as a multiple two-dimensional problem, and the gravity wave spectrum in a given azimuthal direction depends on the heating and mean wind projection in that direction.

2) Mechanical oscillator: oscillating updrafts and downdrafts about a level of neutral buoyancy (LNB) (e.g. the top of the boundary layer, tropopause) perturb the stably-stratified atmosphere at and above the top of the convective motions. For deep, moist convection, updrafts often overshoot their LNBs (i.e. the tropopause), potentially forcing vertically-propagating GWs. Transience in convective updraft strength can perpetuate this forcing. These oscillations can produce upward propagating waves in a manner similar to a mechanical oscillator in a stratified fluid (Clark et al. 1986, Fovell et al. 1992). Some studies have found this oscillator mechanism to dominate GW generation (e.g. Lane et al. 2001), whereas others found thermal and mechanical forcing terms are both equally important (Song et al. 2003). In the set of nonlinear equations, flux terms couple the thermodynamic and momentum equations, and the nonlinear momentum term can oppose the heat source giving some apparent cancellation (Pandya and Alexander 1999, Chun et al. 2008).

3) Obstacle effect or moving mountain: in this mechanism, the top of a convective element acts as a barrier to the background mean flow, producing upstream propagating waves in a manner similar to flow over a mountain (Clark et al. 1986, Pfister et al. 1993). Vertical wind shear, at least near the tops of the convection, is required for this mechanism. The

non-zero net vertically-propagating GW momentum flux is fundamentally derived from the convective momentum fluxes, as convective updrafts vertically transport air parcels with low (high) momentum into regions of high (low) above. Waves generated by the obstacle effect are not stationary relative to the ground as in the case of mountain waves, but rather have horizontal phase speeds similar to the horizontal speed of the convection.

Gravity waves generated by a thermal forcing (proxy for convection) are shown in Figures 1c,d and supplementary Animation 3. Figure 1c and left panel of Animation 3 show that gravity waves propagate away from the convective source in nearly concentric circles spreading away from the source as they propagate upward. In a x-z cross-section (Figure 1d and right panel of Animation 3), convectively generated gravity waves form a fan-like structure with a broad spectrum of wave phase speeds, and horizontal and vertical wavelengths. In this particular simulation, westward propagating waves are not as apparent at z = 85 km, due to much slower vertical group velocity (8) and dissipation in the stratosphere, resulting in asymmetry in Figure 1c. The eastward propagating waves have higher intrinsic phase speeds in the stratosphere and lower mesosphere, propagate upward more quickly, and break in the mesopause region where the mesospheric winds shear brings the environmental winds close to the phase speeds of these eastward propagating waves (Figure 1d).

11.1.4 Gravity waves generated by fronts and jets

Fronts and jets are another major source of GWs in the atmosphere and a significant source of GWs in mid-latitudes. GWs from front/jet systems have been observed on numerous occasions (e.g.: Uccellini and Koch, 1987, Sato et al. 1994, Plougonven et al. 2003, Wang and Geller 2003, Zhang and Yi, 2005, 2008)) and simulated with numerical models (Zhang and Fritsch 1988, Schmidt and Cotton 1990, Jin 1997, Powers and Reed 1993 , Kaplan et al. 1997, Zhang and Koch 2000, Zhang et al. 2001, 2003). Jets/fronts generate mesoscale and low-frequency gravity waves (inertia-gravity waves), for which the rotation of the Earth has an influence and the frequency is of the order of the Coriolis parameter, f. Wei and Zhang (2014), for example, examined gravity waves in moist baroclinic jet–front systems with varying degrees of moisture and found the gravity waves to have horizontal scales between 50 and 500 km, vertical scales between 1 to 6 km, and frequencies of 1 to 15 $\times 10^{-4}$ s^{-1} (periods of 1 to 17 hrs). Most intense gravity wave activity has been observed and modeled near the vicinity of the maximum of the jet velocity (strong curvature of the jet) (Plougonven et al., 2003) and in the exit region of upper-tropospheric jet streaks (e.g.: Guest et al. 2000, Zhang et al. 2001, 2003, Zhang 2004, Wu and Zhang 2004).

The generation mechanisms of gravity waves generated by jet/front systems are still not well understood. Plougonven and Zhang (2014) present a complete review of possible generation mechanisms by such systems. Below, three dry-idealized mechanisms that are thought to be most important are described, two of which form the basis of gravity wave source parameterizations described in subsequent sections:

1) Spontaneous imbalance adjustment (see 3.1 of Plougonven and Zhang 2014): Spontaneous imbalance adjustment is considered a generalization of geostrophic adjustment. In this mechanism, GWs are generated and radiated away as some initially

imbalanced flow comes back into balance. This concept does not address the cause of the initial imbalance, but only considers the GW emission during the evolution back toward some (e.g. geostrophic, cyclogeostrophic) balance. This mechanism is responsible for emission of large-amplitude inertia-gravity waves in regions of strong horizontal curvature of the wind where the flow becomes unbalanced (Fritts and Luo 1992, Luo and Fritts 1993). The residual of the nonlinear balance equation is found to be a useful quantity in diagnosing regions of flow imbalance and predicting regions of wave generation (Zhang et al 2000, 2001, Zhang 2004). Readers are also referred to the review by Ruppert et al. (2021) on this topic.

2) Adjustment emission (see 3.2-3.4 of Plougonven and Zhang 2014): in this mechanism well-balanced flow more continuously radiates GWs during the course of its near-balanced evolution. An early example of such physics was presented by Lighthill (1952), where acoustic waves are generated within fluids by turbulent motions. Adjustment emission has successfully replicated the salient characteristics of gravity waves emitted from vortices and jets in the shallow water model (e.g., Ford 1994a, Ford 1994b, Sugimoto et al. 2008) and in a stratified fluid (e.g., Plougonven and Zeitlin 2002; Schecter 2008). Transient generation in sheared disturbances describes how the evolution of potential vorticity anomalies in a sheared flow leads to a transient generation of gravity waves, which has been discussed in horizontal (Vanneste and Yavneh 2004) and vertical shear (Lott et al. 2010).

3) Shear instability: in this mechanism gravity wave emission occurs via nonlinear interaction between Kelvin-Helmholtz instability and propagating modes (Bühler et al. 1999, Scinocca and Ford 2000). Shear instability is usually considered by neglecting the Coriolis effect. This mechanism of wave generation can occur in very intense shear layers near the surface or at upper levels, above tropopause jets. Kelvin-Helmholtz instability occurs on very small scales (hundreds of meters in the vertical and tens of kilometers in the horizontal), hence in order for gravity waves to propagate upwards, nonlinear emission on the envelope scale (i.e. scale characterizing the extent of K-H instabilities and mean-flow influence) must occur (Fritts 1984, Chimonas and Grant 1984).

Convection often occurs in association with a frontal system and can provide an additional source of GWs and/or influence the generation of GWs by frontal/jet system. Many earlier studies of GWs generated by fronts focused on dry idealized baroclinic wave simulations (e.g., Zhang 2004), however the role of moisture can potentially be very important (Powers 1997, Zhang et al. 2001, Lane and Reeder 2001). Complementary to the work of Zhang (2004), Wei and Zhang (2014), using cloud permitting mesoscale baroclinic system simulations, showed that moisture enhances GW amplitudes and generates additional wave modes in comparison with a dry simulation. Furthermore, based on the study of GWs spectral characteristics using multidimensional discrete Fourier transforms, Wei et al. (2016) further demonstrated that the dry jet/front GW source generates a relatively narrow and less symmetric power spectrum centered around lower phase speeds and horizontal wavenumbers, whereas the moist gravity wave source generates a broader and more symmetrical power spectrum, with a broader range of phase speeds and horizontal wavenumbers. Generation of GWs in frontal systems with a lot of moisture is still a subject of recent research, and diabatic forcing could be a more important generation mechanism. The role of moisture in producing significant momentum fluxes from front/jet systems has been emphasized by many studies (e.g., Plougonven et al. 2015; Wei et al. 2016; Holt et al. 2017).

GWs generated by idealized weak moist baroclinic jet-front systems are illustrated in Figure 1e,f and supplementary Animation 4. As the upper level baroclinic jet develops, with an accompanying deepening surface cyclone, the lower stratospheric (12-km altitude) flow shows a well-recognized pattern of convergence upstream of the trough and divergence downstream of the trough (Figure 1e, and left panel of Animation 4). GW generation begins first with weak amplitude mesoscale GWs appearing in the jet entrance region upstream of the upper level trough, along the surface warm front. As the system matures, mesoscale GW generation occurs primarily in the jet exit region, downstream of the trough and above the surface frontal system (Figure 1f, right panel of Animation 4). In addition, based on a series of four-dimensional ray-tracing experiments, Wei and Zhang (2015) investigated the propagating wave characteristics and the potential source mechanisms of several identified lower-stratospheric GWs in this particular idealized simulation. It was further demonstrated that moist convection may force new wave modes, modify/enhance the existing dry jet/front wave modes through latent heat release, and/or modify the new/existing waves through modification of large-scale flow.

11.1.5: Secondary wave generation

An understudied aspect of the GW lifecycle and a likely underestimated GW source is secondary wave generation (e.g. Bacmeister and Schoeberl 1989), which is generation of GWs by the momentum deposition of a dissipating primary GW. While the research on secondary GW generation, propagation, dissipation, and impact is relatively nascent, there is a growing body of literature on the topic. Currently, at least two secondary GW generations mechanisms have been explored:

1) Large-scale secondary GW generation by localized momentum deposition, or body forces, resulting from a primary GW. The body forcing and secondary GW generation occurs at scales larger than the horizontal scales of primary GW activity. The body forcing from these primary GWs can be both dissipative (e.g. where small-scale instabilities dissipate the wave) and non-dissipative (e.g. a sometimes reversible forcing on a layer as a GW transiently propagates into and out of it). The latter effect is sometimes referred to as “self-acceleration” (e.g. Fritts and Dunkerton 1984). Dissipative secondary GW generation is the focus of Vadas et al. (2003) and Vadas et al. (2018). Wilhelm et al (2018) has investigated the non-dissipative, resonant radiation of mesoscale inertia-gravity waves by a horizontally as well as vertically confined submesoscale gravity wave packet that propagates vertically. It is known from long-short-wave interaction theory (Tabaei and Akylas 2007; Van den Bremer and Sutherland 2014) that such a packet of small-scale waves is able to generate a mean flow consisting of mesoscale wave structures connected to a resonance mechanism, wherein the vertical phase velocity of the emitted long waves match the vertical group velocity of the small-scale gravity wave packet, which acts as a traveling wave source.

2) Secondary GWs are also generated on scales smaller than the horizontal scales of the primary GW activity. Numerous small-scale instabilities can take place during GW breaking and dissipation. Non-linear dynamics can transfer energy from these small-scale instabilities to larger scales that can force a propagating GW (Franke and Robinson 1999). Instabilities can occur inhomogenously within a wave field (e.g. in particular phases where stratification is reduced, or unstable, where wind shear is increased), also forcing waves at scales smaller than wave field (Satomura and Sato 1999, Holton and Alexander 1999, Lane and Sharman 2006, Fritts et al. 2006, Chun and Kim 2008, Heale et al. 2017, Bossert et al. 2018).

At this time, the understanding of secondary GWs is limited; their contribution to the energy and momentum budget of the atmosphere is not well understood, nor represented in weather and climate models that do not resolve the relevant mechanisms.

11.1.6: Gravity wave propagation and dissipation

GW characteristics change as they propagate through an atmosphere with changing buoyancy frequency and mean wind, as suggested by (2). As a GW propagates upward through wind shear that is opposite to the wave's propagation direction, the vertical wavelength of the wave will increase. Similarly, the vertical wavelength of the wave will decrease when the wave propagates through wind shear in the same direction as the wave propagation. If wind in the direction of the wave propagation changes so that $\omega^* = \omega - Uk$ reaches zero, a 'critical level' is reached. This is the level at which the horizontal phase speed, c_x, matches the background wind. As a GW approaches a critical level, linear theory predicts the wave vertical wavelength goes to zero, zonal wind perturbations go to infinity, and the wave steepens and overturns. Prior to reaching the critical level, however, instabilities (e.g. K-H, static instability) are typically triggered that dissipate the wave, ending its vertical propagation. This is illustrated in the top panel of Figure 2, which shows a wave packet propagating upward and in the positive x direction into a region of increasing zonal mean wind (in the same direction as the wave propagation). As the wave packet propagates upward, its vertical wavelength decreases as it approaches the critical level near t = 7500 and altitude of ~ 75 km, and the GW packet dissipates.

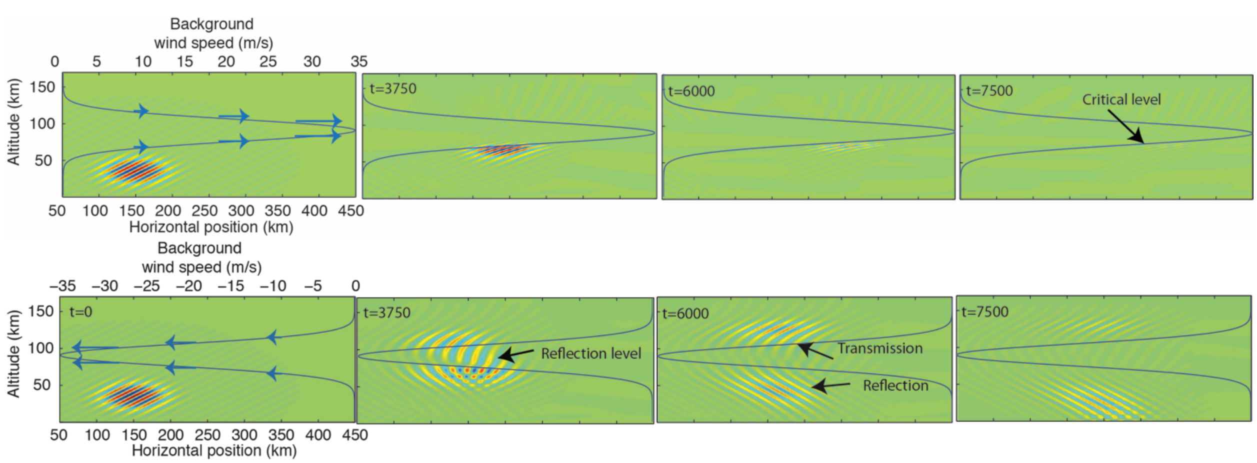

Figure 2: Simulated propagation of a gravity wave packet through two different vertically varying background winds (top and bottom) at four different times (from left to right) using the MAGIC model (Snively and Pasko 2008). The top panel shows a packet propagating in the same direction as the background wind flow (indicated by the black line), which approaches a critical level at ~80km and is then absorbed into the mean flow. The bottom panel shows the same packet propagating against the background wind flow. In this case, the wave encounters a turning point (reflection) level and partial transmission and reflection occur. The color indicates the perturbation horizontal wind associated with the gravity wave packet. Times of the simulation in seconds is depicted in top left corner of the panels. Adapted from Heale and Snively (2015).

When such a wave packet propagates into a region where the wind speed through the wave increases, the intrinsic phase speed and frequency both increase. According to (2), the wave packet can reach a level where the intrinsic frequency matches the environmental buoyancy frequency and the vertical wavelength approaches infinity. This level is referred to as a turning or reflection level, as at least partial GW reflection occurs here. Above the reflection level, m is imaginary and wave evanesces, or decays, exponentially with height. This situation is illustrated in the bottom row of Figure 2. Where a wave packet is propagating upward and in the positive x direction with shear against the direction of propagation above the wave. As the wave packet approaches the reflection level, the phase lines become more vertically oriented. At t = 3750 s, both upward and downward portions of the wave packet superpose to produce the wave field below the reflection level. Above the reflection level, nearly vertical phase lines are seen, with a portion of the wave perturbations decaying with height. The wave does not decay above the reflection level immediately. In this case, the wave maintains enough amplitude to "tunnel" through this evanescent layer into the slower winds aloft that allow vertical propagation once again (e.g. Mixa et al. 2021). In this case, part of the wave packet was reflected at the reflection level, while part was able to tunnel through the evanescent layer and continue propagating upward.

Another important characteristic of GWs is how their amplitudes grow with height, even in an environment that is constant in height. Linear, 2-D GWs in a horizontally uniform background have a constant vertical flux of horizontal momentum (e.g. $\bar{\rho}\overline{u'w'}$) with height (e.g. Eliassen and Palm 1960). As density decreases exponentially with height, this requires the GW perturbations to grow exponentially with height. Similar to encountering a critical level, eventually, wave amplitudes become large and trigger instabilities that dissipate the wave.

11.1.6: Gravity wave impacts

Both energy and momentum are extracted from the mean flow, or via interaction with topography, when GWs are generated. Propagating GWs transport this energy and momentum, depositing them wherever the waves are dissipated. While both are important, the energy extracted, transported, and deposited is typically neglected. The momentum, however, is not neglected and represents an important forcing on the background horizontal flow.

MWs attain their momentum flux and drag through interactions with orography. Vertically-propagating MWs induce positive pressure perturbations upstream of the mountains and negative perturbations downstream during generation, resulting in a net horizontal pressure force by the atmosphere on the mountains. The mountains exert an equal and opposite force on a lowest layer of the atmosphere. This low-level layer than perturbs a layer immediately above and a pressure drag by the layer above is exerted on this low-level layer. If no MW dissipation occurs, the forces by the mountain and the layer above on the low-level layer cancel, resulting in no net horizontal force on this layer. Layers increasingly perturb layers above, propagating the MW upward and fluxing atmospheric momentum downward. When the MW dissipates, the top of the dissipation layer is no longer displaced by the primary MW. Atmospheric momentum above the dissipation layer no longer balances the momentum fluxed out the bottom of this layer, and a net force is exerted on the flow. In short, MW drag is exerted wherever the MW is dissipated is fundamentally a reaction to pressure forces by the atmosphere on mountains.

While the forcing exerted by non-orographic GW dissipation technically comes out of thin air, it does come from somewhere. In general, non-orographic GWs attain the momentum and energy they flux from the flow in which they were generated and then spatially redistribute the energy and momentum within the atmosphere. Wave fields generated by non-orographic GW fields tend to be more complex than MWs, having both a spectrum of spatial scales and a spectrum of phase speeds and intrinsic frequencies. For example, in the absence of environmental shear, GWs radiate away from moist convection symmetrically in all directions. While the eastward-, westward-, northward-, and southward-propagating GWs all flux momentum, the net vertical flux of zonal and meridional momentum by these GW beams cancel, resulting in net zero momentum flux. While the net momentum fluxes are zero at the source level, wind shear aloft forces the different beams of GWs to encounter critical levels at different altitudes and exert forces on flows in different directions at different altitudes. Such a phase speed spectrum is critically important in forcing the quasi-bienial oscillation and semi-annual oscillation in the tropical stratosphere.

While the previous discussion suggests convective GWs are symmetric, they rarely are in reality, having a preferred propagation direction and a net momentum flux due to the fact that convection often occurs in environments with shear. Wind shear both allows there to be flow relative to the tops of the convection and allows convection to transport low-momentum air from low lower-levels and act as a barrier to the flow across the top of convection. The convective momentum fluxes are likely important in determining a portion of the convective GW spectrum.

GWs generated by jets and fronts derive the energy and momentum they flux from the various imbalances that are produced as the systems evolve in time. The GWs are generated by these imbalances and adjust the flow in the direction of balance.

Quantitatively, the influence by GWs on the zonal momentum appears when deriving an equation for a background or, traditionally, a Reynolds-averaged horizontal wind. These equations that govern a larger-scale horizontal flow contain the following term, representing the influence of the vertical convergence of the vertical flux of horizontal momentum on the background horizontal flow:

$$\boldsymbol{GWD} = \frac{1}{\bar{\rho}}\frac{\partial}{\partial z}\left(\bar{\rho}\overline{u'w'}, \bar{\rho}\overline{v'w'}\right) \qquad (10)$$

Where $\bar{\rho}$ is the background atmospheric density, u', v', and $w'$are the horizontal and vertical perturbation velocities, and the overline operator, $\overline{(.)}$, is a linear background operator of some kind (e.g. a low-pass filter) used to define the background flow. This term is defined as GW drag (GWD) and has units of acceleration or drag force per unit mass. While momentum fluxes and their divergences are obviously relevant to forcing of the background momentum, pseudomomentum is more relevant to GW dynamics, and its divergence is sometimes used to quantify GW influences on the mean flow (see Wei et al. 2019 for a comparison of these approaches).

The momentum fluxed and deposited by GWs is significant in Earth's general circulation, especially in the stratosphere, mesosphere and lower thermosphere. Since GWs grow in amplitude with height, and background horizontal momentum (e.g. $\bar{\rho}\bar{u}$) decreases with height, the importance of GWs in the general circulation tends to increase with height. In the lower- to mid-troposphere, GWs have less influence on large-scale momentum but are still important in initiating convection and convective organization (Bretherton and Smolarkiewicz 1989, Pandya and Durran 1996, Shige and Satomura 2000, Lac et al. 2002, Fovell et al. 2006, Lane and Zhang 2011, Su and Zhai 2017, Ruppert et al. 2021). In the upper troposphere and lower stratosphere, GWD does become important in the zonal mean climate (Palmer et al. 1986, Bacmeister 1993, Butchart et al. 1998). In the tropical stratosphere, gravity waves contribute 50 to 90% of the forcing of the Quasi-biennial Oscillation (QBO) (Kawatani et al. 2010, Alexander and Ortland 2010, Richter et al. 2014, Geller et al. 2016, Bushell et al. 2020). In climate models, GW parameterizations largely determine the period and frequency of the QBO, and most models without a gravity wave parameterization won't be able to produce a QBO (Giorgetta et al. 2006, Richter et al. 2014, Geller et al. 2016, Butchart et al. 2018). The representation of the QBO in climate models is becoming more important as impacts of the QBO on the tropospheric variability are becoming clearer (Giorgetta et al. 1999, Yoo and Son 2016, Wang et al. 2018). GWs also contribute to the driving of the semi-annual oscillation (SAO) (Hitchman and Leovy 1988, Ray et al. 1988, Richter and Garcia 2006) and the Mesospheric Semi-Annual Oscillation (MSAO) (Dunkerton, 1982).

In the extratropical stratosphere, GWs provide a portion of the driving of the Brewer Dobson circulation, especially during the spring-to-summer transition season in each hemisphere (Alexander and Rosenlof 1996, Rosenlof 1996, Alexander and Rosenlof 2003, Okamoto et al. 2011, de la Camara et al. 2016). MW drag peaks in the upper stratosphere and mesosphere, (e.g. Kruse 2020), and together with other extratropical GWs, largely from fronts and jets, control the state of the polar stratospheric temperatures and strength of stratospheric polar night jet, (Boville 1991, Garcia and Boville, 1994). Inadequate representation of GW drag in general circulation models can lead to a cold bias of southern winter stratosphere temperature in the polar region (e.g.: Austin et al. 2003, Eyring et al. 2007, McLandress et al. 2012). One of the largest effects that GWs have on the atmosphere occurs in the mesosphere. Non-orographic GWs dominate GW drag here and deposit net westward momentum in the winter mesosphere and net eastward momentum in the summer hemisphere causing the reversal of the zonal mean jets and driving a mean transport circulation from the summer to winter hemisphere, leading to a warm winter and cold summer mesopause (Lindzen 1981, Holton 1982, 1983, Garcia and Solomon 1985).

Waves that are not filtered by critical levels, reflected by turning levels, and do not break in the middle atmosphere will be dissipated in the thermosphere by increasing molecular viscosity and thermal conductivity or, in polar regions, ion drag. The damping rate is inversely proportional to the vertical wavelength (Walterscheid and Hickey 2011) so waves with larger vertical wavelengths (and phase speeds) can propagate higher into the thermosphere before dissipating (Vadas and Fritts 2005, Vadas 2007, Vadas and Nicholls 2012, Heale et al. 2014, 2018). However, spectra of wave packets that propagate into the thermosphere from below often evolve from longer to shorter vertical wavelengths in time as a result of dispersion. This occurs because the longer, faster vertical wavelength components reach the thermosphere, and are dissipated first, while the shorter, slower components arrive later (Heale et al. 2014, 2018). The dissipation of these waves produces local body forcing and heating/cooling of the thermosphere (Miyoshi et al. 2014, Yiğit and Medvedev 2009, Yiğit et al. 2009, Vadas et al. 2014, Hickey et al. 2011) and will also generate secondary waves (Vadas et al. 2018). It is suggested that wave dissipation in the thermosphere leads to a drag that opposes the mean zonal winds and is stronger at high latitudes (Miyoshi et al. 2014) and in the winter hemisphere (Yiğit et al. 2009). Thermospheric dissipation of waves from deep convective sources can also lead to in-situ generation of planetary-scale diurnal and semidiurnal tides (Vadas et al. 2014). Waves that reach the thermosphere can also couple to the ionosphere, producing travelling ionospheric disturbances (e.g. Liu and Vadas 2013, Azeem et al. 2017, Yu et al. 2017) and ion outflow (Burleigh et al. 2018). Compared to other regions of the atmosphere, the impacts of waves in the thermosphere are still unknown and require further investigation.

11.2 Representation in large scale models

11.2.1 History and basic components

The need for representing GWs in General Circulation Models (GCMs) began with the recognition of ‘missing drag’ in such models. Without explicit drag in the middle atmosphere, if the atmosphere was in radiative equilibrium, the polar night jet in the stratosphere in models would be much stronger than observed and the winter (summer) mesopause would not be warm (cold). Early GCMs which extended to the stratosphere and mesosphere often used Rayleigh friction to provide a crude parameterization of the effect of breaking gravity waves in the mesosphere and were able to reproduce the observed features of the zonal mean wind and temperature in the stratosphere and mesosphere (e.g.: Boville 1986). First implementations of GW parameterizations in GCMs focused on representing GWs generated by orography (Boer et al. 1984, Palmer et al 1986, McFarlane 1987). Subsequently, parameterizations in GCMs were extended to include representation of non-orographic GWs (Rind et al. 1988, Fritts and Lu 1993, Medvedev and Klaasen 1995, Hines 1997a,b, Alexander and Dunkerton, 1999, Warner and McIntyre 2001).

GW parameterizations in GCMs have three basics components: (1) specification of waves at the source levels, (2) wave propagation with height, and (3) wave dissipation, from which momentum deposition to the mean flow is estimated. Parameterization of MWs is traditionally distinguished from non-orographic GWs, with the horizontal phase speed of orographic MWs assumed to be zero, while non-orographic GWs have a spectrum of phase speeds. Hence, MW drag has historically been treated separately, and this distinction generally remains today. The source spectra of non-orographic waves initially were specified to be uniform in space and time in the first implementations of parameterizations in GCMs. Spatially-uniform sources continue to be standard practice in many GCMs (e.g.: Scinocca et al. 2008, Adachi et al. 2013, Davini et al. 2018). However, in recent years, separate source spectrum parameterizations have been developed for waves generated by convection and fronts, and these are described in section 12.2.3. These source spectra parameterizations replace the arbitrary/globally defined non-orographic source spectra in GW parameterizations even though they still carry large uncertainties.

11.2.2 Description of GW Parameterizations

The primary function of GW parameterizations as currently applied in global models is to compute the wave-driven force on the mean flow. The mean flow in this context is the grid-box mean, and the waves are meant to represent sub-grid, or otherwise unresolved, GW anomalies. The essential ingredients of GW parameterizations include specification of input parameters describing the gravity wave sources, estimation of the wave dissipation as a function of height, and output vertical profile of the vector momentum forcing via (10). The wave dissipation profile implies an energy dissipation rate profile and, in some models (e.g. the Whole Atmosphere Community Climate Model, Gettleman et al. (2019)), this energy dissipation is tied to vertical mixing of trace gases. Conversion of energy dissipation to vertical mixing is not direct, however, because the mixing may be more or less perpendicular to isentrope and tracer gradients (Lelong and Dunkerton 1998) and so must be scaled by an uncertain Prandtl number, with values O~1-100 (Smith and Brasseur 1991).

GW parameterizations typically start with some specification of the wave stress or momentum flux along with the wave propagation properties (wavenumbers, phase speeds, propagation directions) at a source level, which is selected to be somewhere between the surface and the 90 hPa (e.g. near the terrain for MWs and upper troposphere and lower stratosphere for non-orographic GWs). The vast majority of GW parameterizations assume GWs propagate only vertically and instantaneously through the column of atmosphere above the source level. Two notable exceptions are Amemiya and Sato (2010), where 3-D GW propagation was accounted for, and Eckermann et al. 2015b, which accounted for lateral spreading of MW activity and how this influenced MW amplitude and breaking levels. Wave dissipation is estimated with a variety of techniques depending on the parameterization. The plane wave assumption is always made, so the flux and force both lie along a specified direction of wave propagation. This direction is specified at the wave source level and is assumed to remain constant through the column until the wave is completely absorbed. Thus, gravity wave parameterizations are one-dimensional (vertical), utilizing parameters and model fields that are projected along the direction of wave propagation. The output force is applied to the vector momentum equations by projection onto zonal and meridional directions.

Differences among parameterizations include (a) specification of the sources, and (b) assumptions that control the wave dissipation with height. For dissipation, Lindzen's (1981) saturation theory, with modifications formulated by Holton (1982), forms a starting point for most parameterizations currently in use. Here, parameterized waves are treated as individual steady hydrostatic monochromatic plane waves. Using (2), the continuity polarization relation

($k\hat{u} = -m\hat{w}$), and the fact that momentum flux for such idealized plane waves is constant in height, the following non-dimensional wave amplitude, which quantifies both non-linearity and wave steepness, can be derived:

$$\frac{\hat{u}}{|U-c|} = \left(\frac{2\, MF_{src}\, N}{\bar{\rho}|U-c_{px}|^3 k}\right)^{\frac{1}{2}} \qquad (11)$$

where hatted quantities are the sinusoidal amplitudes. Here MF_{src}, k, and c_{px} are constant in height. Changes to this non-dimensional GW amplitude in height result from changes in $\bar{\rho}$, N, and $|c_{px}^*| = |U - c_{px}|$. When this non-dimensional amplitude is small, the GW is linear and the steepness of the wave, as predicted by this linear theory, is low. As a GW propagates upward, density decreases exponentially, and so wave amplitude increases exponentially. Increased stratification and environmental wind shear that brings the wind closer to the phase speed can both force GW non-linearity.

When the non-dimensional amplitude, (11), exceeds unity, linear theory predicts the wave will loft dense fluid over light fluid and induce static instability. The saturation hypothesis (Lindzen 1981) assumes instabilities (e.g. static, Kelvin-Helmholtz instabilities) continuously and instantaneously prevent the GW from exceeding some non-dimensional wave amplitude (e.g. unity for static instability). For example, if a GW is propagating upward in shear that brings the environment closer to its phase speed (i.e. as it approaches a critical level), the wave amplitude grows. Eventually, this critical wave amplitude is reached. Then, the momentum fluxed by the GW is reduced such that (11) gives the critical non-dimensional wave amplitude. The momentum flux is reduced with height when the wave is saturated, the vertical derivative of which gives the forcing to the mean flow. If the wind shear reverses so that the intrinsic frequency increases and the non-dimensional GW amplitude is reduced below the critical amplitude, then the GW once again propagates upward conserving its momentum flux and exerting no force on the mean flow.

Other parameterizations in use in global climate models today make different wave dissipation assumptions. Alexander and Dunkerton (1999) represent a finely-resolved spectrum of discrete, independently treated, monochromatic waves and assumes complete annihilation of an individual wave at its breaking level (Alexander and Dunkerton 1999). Hines (1997a,b) proposed a "Doppler Spread" mechanism, assuming that nonlinear interactions among waves in the spectrum reshape the spectrum with altitude. (See McLandress 1998 for a concise summary of the application of the Hines (1997a,b) parameterization.) Warner and McIntyre (2001) assumes a similar reshaping of the spectrum with altitude but based on the empirical observations of the shape, coupled to Lindzen's wave saturation concept. Both the Hines and the Warner and McIntyre approaches assume a particular vertical wavenumber spectrum shape at the source level. A more in-depth overview of such spectral parameterizations not using the conventional saturation concept above is provided in Medvedev and Yiğit (2019).

11.2.3 GW Source Parameterizations

11.2.3.1 Orography

Specification of MW sources is rather simple in most GCMs. The first formulations prescribed only a single, monochromatic vertically propagating wave with zero horizontal phase speed (Boer et. al 1984, Palmer et al. 1986, and McFarlane 1987), and these formulations are still being used in most GCMs. The GW source specifications are based on 2D theory assuming hydrostatic, steady, horizontally uniform flow over an obstacle. Wave amplitudes at the source levels are defined based on a measure of subgrid-scale orographic variance. In early orographic GW parameterizations, the surface stress vector is parallel to and opposite of the mean flow at the lowest level of the model, assuming isotropic unresolved topography.

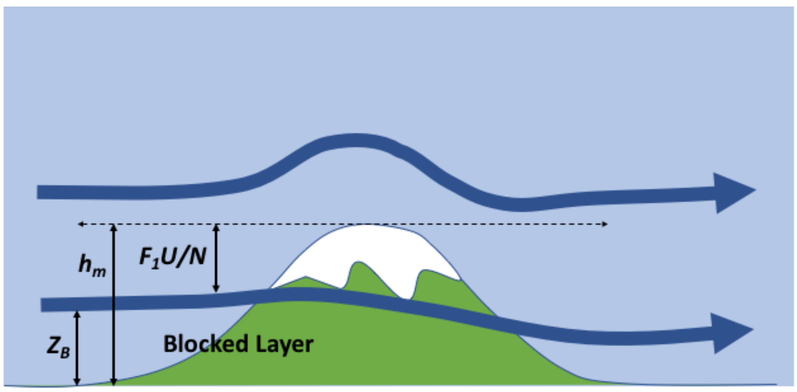

Figure 3: Schematic depiction of flow over and around a large mountain following Lott and Miller (1997). h_m is the height of the mountain, Z_B is the height of the blocked layer. Blocked flow can develop if the mountain height exceeds $F_1(U/N)$(see text).

The first orographic gravity wave drag schemes (e.g. Palmer 1986, McFarlane 1987) neglected the impact of topographic anisotropy and did not consider drag produced by nonlinear dynamics near the surface (e.g. downslope winds, blocking, flow splitting), which can lead to large amplification of surface stress and hence be important to general circulation (e.g.; Pierrehumbert and Wyman,1985, Baines and Palmer, 1990, Sandu et al. 2019). Lott and Miller (1997) described an orographic drag parameterization that incorporated the impact of near-surface nonlinearities due to flow diversion around obstacles (also referred to as blocking). The key elements in their approach are schematically illustrated in Figure 3. When mountain heights h_m exceed a critical value $F_1\left(\frac{U}{N}\right)$ a portion of the flow is assumed to be diverted or blocked. The depth of this layer is given by:

$$Z_B = Max(h_m - F_1\frac{U}{N}, 0) \qquad (12)$$

The parameter F_1, a critical non-dimensional mountain height or vertical displacement, is known from numerical and tank experiments to be of order 1 but may depend on obstacle shape. The forcing amplitude for vertically-propagating gravity waves in Lott and Miller (1997) is taken to be the full mountain height, however they suggest that this should be reduced to something approaching $F_1(U/N)$ in three dimensional flows.

Within the blocked layer, Lott and Miller (1997) assume the drag follows a bluff-body law:

$$\frac{\partial U}{\partial t} \propto -\frac{1}{\bar{\rho}}\frac{\partial(\bar{\rho}\,\overline{u'w'})}{\partial z} = 0.5\,\bar{\rho}\,C_d\,l(z)U|U| \qquad (13)$$

Where C_d is a nondimensional drag coefficient close to 1 and $l(z)$ is the cross-stream length presented by the obstacle. Lott and Miller (1997)'s formulation still employs a single wave.

The Scinocca and McFarlane (2000) parameterization employs two, instead of one, vertically propagating waves in order to provide a representation of the azimuthal distribution of momentum flux in the parameterized gravity-wave field launched by a 'best-fit' elliptical barrier, similarly to Lott and Miller (1997), but with a new way of defining unresolved topography. Scinocca and McFarlane (2000) also extended the representation of low-level drag to include enhancement by the downslope windstorm regimes. These flows are analogous to hydraulic supercritical flow (Smith 1989) and are thought to be related to near-surface wave breaking (e.g. Clark and Peltier 1977, Bacmeister and Pierrehumbert 1988). Three dimensional numerical studies cited by Scinocca and McFarlane (e.g.; Miranda and James 1992, Olaffson and Bougeault 1996) suggest that downslope winds with enhanced drag appear for a limited range of mountain heights, roughly for $F_1 < Nh_m/U < 3F_1$. In these flows the surface drag applied in the scheme is determined by

$$\tau_{sfc} = (1+\beta(F))\tau_{lin} - \tau_c \qquad (14)$$

where τ_c is the moment flux carried by the freely propagating waves and τ_{lin} is the nominal linear wave drag $\sim\rho NUh_m^2/L$. This enhanced drag is applied via a linearly decreasing momentum flux profile in a layer from the surface to the first breaking level above the mountain. The height of this breaking level is approximated using linear theory. The enhancement factor $\beta(F)$ peaks around $F = Nh_m/U = 1.5F_1$ and has values between 2 and 4 depending on obstacle geometry. This parameterization of form drag can change the direction of the low-level flow to be more parallel to unresolved topographic ridges.

A new approach to orographic GW source parameterization is presented by van Niekerk et al. (2021), where they use the spectral, hydrostatic linear MW theory of Garner (2005) and Smith and Kruse (2018). Here, a two by two matrix of orographic GW drag coefficients are computed from the 2-D Fourier transform of the subgrid-scale terrain. Multiplication of the source-level wind vector with this drag matrix produces a source MW momentum flux vector that takes into account all subgrid scales and orographic anisotropy, eliminating the monochromatic assumption common to all previous MW drag parameterizations, at least at the source. Van Niekerk et al. (2021) further develop a parameterization for how the elements of the drag coefficient matrix depend on low-level blocking. Initial implementation in the Met Office Unified Model demonstrates this approach does a much better job at keeping total GW drag (resolved + parameterized) constant as grid resolution is changed relative to previous monochromatic parameterizations and improved weather prediction performance.

11.2.3.2 Convectively generated gravity waves

Source spectra parameterizations for convectively generated gravity waves were developed on the basis of the three dominant generation mechanisms: thermal forcing, mechanical oscillator, and obstacle effect (described in detail in Section 11.1.3). Rind et al. (1988) was first to implement a parameterization for nonstationary GWs linked to wave sources. The parameterization included waves generated by convection and wind shear based on theoretical assumptions. GW momentum flux of convectively generated GWs was related to the convective mass flux generated by the model. The phase speed of gravity waves was set to the mean wind over the convective region +/- 10 m s^{-1}, and for deeper convection additional waves with phase speeds equal to the mean wind +/-20 m s^{-1} and +/-40 m s^{-1} were added. Kershaw (1995) developed a convective GW source parameterization which can be viewed as a parametrization of the obstacle effect as it focuses on parameterizing the effect of wave generation by flow over heating. A similar parameterization was developed by Chun and Baik (1998) parameterizing the effect of wave generation by mean flow over steady heating, representing only gravity waves that are stationary relative to the heat source. This parameterization was further extended to include effects of vertical wind shear by Chun and Baik (2002).

Beres et al. 2004 and Beres 2004 developed a parameterization of convectively generated GWs assuming that thermal forcing is the dominant GW generation mechanism. This method is based on linear theory and both steady and oscillatory components of the heating, are considered; hence stationary and non-stationary GWs, relative to the heating, are represented. The dominant spectral properties of the GWs depend on the horizontal and vertical scales of the heating. The dominant GW phase speed is primarily determined by the convective heating depth, h, leading to a dominant wave phase speed of +/- 15 m s^{-1} for $h = 5$km, and a dominant wave phase speed of 25 m s^{-1} for h = 10 km (assuming horizontal scale of heating of 2.5 km). The horizontal scale of the heating primarily changes the amplitude and not the characteristics of the wave spectrum. The momentum flux of convectively generated GWs is proportional to the square of the heating. The effects of environmental wind in and above the convective region are also incorporated into the parameterization, as wind shear can create a large asymmetry in the GW spectrum (Beres et al. 2002). A similar parameterization was developed by Song and Chun (2005) based on a more complex vertical structure of the zonal mean wind and stability.

The convective source parameterizations by Beres et al. 2004 and Song and Chun (2005) based on thermal forcing are a large improvement over fixed source representations as they provide physically based connections between GWs and their evolving tropospheric sources, and hence, respond to changes in convection on all time scales including changes resulting from climate change. However, both of these parameterizations omit the effects of the nonlinear forcing (Chun et al. 2005). Chun et al. (2008) proposed a method of including the effects of nonlinear forcing effect on a spectrum of convectively generated GWs and showed that this inclusion reduced cloud top momentum flux by about 10%, except for middle latitude storm-tracks regions where the cloud-top momentum flux was amplified. Choi and Chun (2011) updated the Song and Chun (2005) parameterization by determining two free parameters of that parameterization: the moving speed of the convective source and the wave propagation direction.

Taking a slightly different approach, Lott and Guez (2013) developed a source spectrum parameterization for convectively generated GWs based on a stochastic approach presented in Eckermann (2011). In this approach, a few monochromatic waves chosen randomly from a probability distribution are launched at each time step. The amplitudes of the waves are proportional to the square of the diabatic heating derived from the precipitation field. This approach leads to a wider range of wave amplitudes, leading to a lower level of momentum deposition as compared to uniform sources. In addition to the complex convective source parameterization described above, Bushell et al. (2015) implemented a relatively simple convective GW source representation by linking GW momentum flux amplitude to the square root of total precipitation. The introduction of the amplitude dependence generated launch-level flux amplitudes with greater spatial and temporal variability, increasing realism of parameterized convectively generated GWs.

The inclusion of all of the above-described convective source parameterizations had a positive impact on simulations of climate in several GCMs. Parameterizations of Chun and Baik (1998) and Chun and Baik (2002) improved the representation of the middle atmosphere in the Yonsei University atmospheric GCM (YONU AGCM; Chun et al. 2001), the National Center for Atmospheric Research (NCAR) Community Climate Model (CCM) version 3 (Chun et al. 2004)], and the National Centers for Environmental Prediction (NCEP) global spectral model (GSM) (Jeon et al (2010)). The Beres et al. (2005) was implemented in Whole Atmosphere Community Climate Model, version 2 (WACCM2) instead of the arbitrarily specified source spectra only in the tropics and resulted in an improved representation of the stratospheric semi-annual oscillation (SAO) (Beres et al. 2005). The Song and Chun (2005) parameterization was implemented in the Whole Atmosphere Community Climate Model, version 1b resulting in an alleviation of the model's zonal mean wind biases, primarily in the low to mid latitudes of the upper stratosphere and the mesosphere, and improving the structure and the magnitude of the SAO (Song et al. 2007). Choi and Chun (2013) demonstrated a reduction in wind biases and alleviation of cold temperature biases in the winter polar stratosphere using the Choi and Chun (2011) spectrum and the ray-based parameterization of Song and Chun (2008). Unfortunately, neither one of these parameterizations remedied the lack of an internally generated QBO in WACCM; However, a decade later, an internally generated QBO was generated with the Beres et al. (2005) parameterization in the Community Atmosphere Model, version 5 (Richter et al. 2014), and subsequently in WACCM (Garcia and Richter 2019) but only after the vertical resolution of these models was doubled to ~ 500 m in the free troposphere and lower stratosphere. The implementation of the Beres et al. (2004) parameterization in the ECHAM6 model led to improvements of several aspects of the QBO. With the Lott and Guez (2013) parameterization, the LMDz model was able to obtain a QBO with vertical resolution in the stratosphere of ~ 500 m. The modifications to the source level amplitudes by Bushell et al. (2015) led to the improved representation of the QBO in the UK Met Office global model.

11.2.3.3 Gravity waves generated by jets/fronts

Parameterizations of GWs generated by jets/fronts are less developed and less common in GCMs as compared to parameterizations of orographic and convective gravity wave sources. As mentioned in the previous section, Rind et al. (1988) parameterized non-orographic GW sources by convection and shear. Shear-generated GWs were launched at jet stream level and assigned a single wavenumber and phase speed in each GCM grid box dependent on the direction of the shear and wind velocity in the shear layers. Wave momentum flux magnitude was set to be proportional to the square of the wind shear between two successive layers. Subsequently, Charron and Manzini (2002) parameterized frontally generated gravity waves. They used the frontogenesis function (Miller 1948, Hoskins 1982) to diagnose the location of fronts. In this approach, GWs were launched at a fixed level of 600 hPa, and if the frontogenesis function exceeded a critical threshold, a relatively high gravity wave variance was imposed in two cross-front directions. At grid points where the frontogenesis function was not exceeded, GWs were launched with a much lower variance representing other possible GW sources. The implementation of this parameterization in the MAECHAM4 model produced a reasonable representation of the stratospheric and mesospheric dynamics. Richter et al. (2010) used a modified version of the Charron and Manzini (2002) approach to represent frontally generated GWs. They also used the frontogenesis function and a launching level of 600 hPa, and only launched frontally generated gravity waves when the frontogenesis threshold was exceeded, and no small amplitude spectrum was employed. In order to obtain enough drag in the stratosphere/mesosphere via this approach, the frontogenesis threshold used was ~ half of that used by Charron and Manzini (2002), however no additional background GW spectrum was used. Richter et al. (2010) used the Beres et al. (2004) convective GW parameterization as well, hence GWs in the Tropics were primarily generated from the convective scheme and in the extratropics from the frontal scheme. When the frontogenesis threshold was exceeded, a Gaussian GW momentum flux phase speed spectrum of constant value was launched. Hence the frontogenesis function was used to produce realistic spatial and temporal variability of frontally generated GWs, including seasonality. However, there was no relation between the properties of fronts and the properties of the GWs generated by them. Figure 4 shows the convective (top panels) and frontal (bottom panels) eastward and westward momentum flux at 100 hPa in the Whole Atmosphere Community Climate Model, version 3.5 (WACCM3.5) used in Richter et al. (2010). The figure clearly shows the dominance of convectively generated gravity waves in the tropics and of frontally generated gravity waves in the extratropics. Convectively generated GWs follow the seasonal cycle of tropical convection, with highest values of GW momentum flux in the NH winter (summer) primarily south (north) of the equator. Although the relationship between the spectrum of waves launched from fronts is not linked to their properties, the 100 hPa momentum flux reflects the seasonal cycle of frontal systems with a maximum in the winter season, and an asymmetry between eastward and westward propagating waves resulting from the strong filtering of eastward propagating GWs by strong tropospheric westerlies between 600 hPa and 100 hPa.

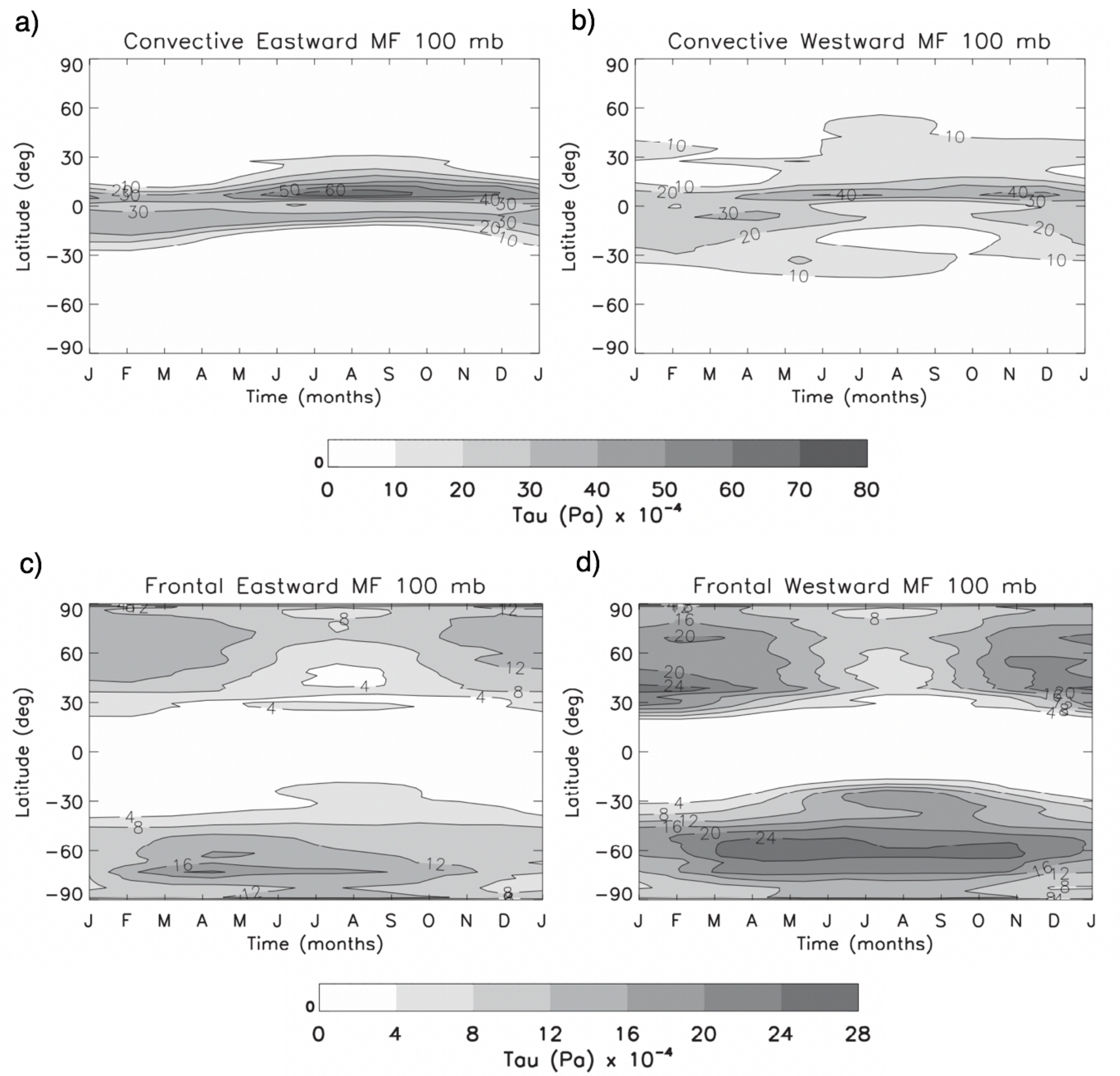

Figure 4: Total eastward (left panels) and westward (right panels) momentum flux (in Pa) for convectively (top panels) and frontally (bottom panels) generated gravity waves as a function of latitude and time of year derived from WACCM3.5. Figure adapted from Richter et al. (2010).

Camara and Lott (2015) parameterized GW generation via spontaneous adjustment mechanism (described in section 11.1.4.) in combination with stochastic approach used in Lott and Guez (2013) to parameterize convective gravity wave sources. In this parameterization GW Eliassen-Palm flux is related to the amplitude and depth of potential vorticity anomalies, hence determining the location and amplitude of GWs. Even though spontaneous adjustment theory predicts exponentially small GW perturbations, the implementation of the scheme in LMDz provided enough extratropical wave drag to obtain reasonable circulations in the stratosphere and mesosphere (Camara and Lott 2015).

11.2.4 Uncertainties and parameter tuning

As GW drag parameterizations are designed, constants are inevitably involved in the derived relations. These constants are not always well constrained and, in practice, are often tuned (more below). Examples include horizontal wavenumber (estimated from unresolved orography in OGW parameterizations, a constant in non-orographic GW parameterizations) and a critical non-dimensional wave amplitude, defining a non-dimensional GW amplitude at which instabilities will begin dissipation. An additional "efficiency factor," e, is typically introduced into GW parameterizations, having values between zero and unity. This term was introduced into early OGW parameterizations in order to reduce excessive MW drag in the lower stratosphere (e.g. Klinker and Sardeshmukh 1992). An efficiency factor is a common part of most GW parameterizations, both orographic and non-orographic. This factor is typically applied in one of two ways: 1) e is multiplied with the drag profile, reducing drag but not influencing the levels where the parameterized wave breaks or 2) just applied to the source-level momentum flux. The latter option reduces the wave amplitude, influencing initial breaking levels and where GW drag is exerted.

A variety of physical justifications for an efficiency factor have been put forward. GWs may occur intermittently within spatial and/or temporal grid scales. There can also be spectral intermittency, where the spectrum that is specified at the source may not be fully represented at all points and times. Mountains are 3-D and not 2-D, as treated by the parameterizations, which can reduce source-level momentum fluxes, as ridges are not necessarily perpendicular to the flow or the mountains represented could be more isolated. These real effects may result in reducing the momentum fluxes and drags below that predicted by the simple 2-D, steady, hydrostatic, instantaneous, Boussinesq, linear, monochromatic, only vertically-propagating, Wentzel-Kramer-Boussinesq theory upon which most GW parameterizations are based.

Ideally, the tuning constants involved should be constrained by observations. However, current observation platforms (aircraft, radiosondes, super-pressure balloons, satellite-borne nadir and limb sounders) have limited capability for quantitatively constraining 3-D GW characteristics and momentum flux globally due to low frequency in space and time and/or lack of sensitivity to the entire spectrum of GWs. Still, progress towards verifying GW parameterizations has been made in recent years with derivations of global GW momentum fluxes (e.g.: Vincent et al. 1997, Ern et al. 2004, Alexander et al. 2008, Hertzog et al 2008, Ern et al. 2017, Hindley et al. 2020). Geller et al. 2013 made a first attempt at comparing parameterized gravity wave momentum fluxes in climate models to gravity wave momentum fluxes derived from observations. This work focused on absolute momentum fluxes (sum over all directions) and showed a general good spatial agreement between models and global satellite estimates, but the observations were not yet able to provide meaningful constraints. Recent measurements from super-pressure balloon campaigns are able to derive GW momentum fluxes with higher accuracy (Jewtoukoff et al. 2013, 2015), but these are limited to a single level in the lower stratosphere, limited in latitude, and limited to campaign periods. Despite new sophisticated methods of analyzing satellite observations and estimating vector momentum fluxes, GW drag on the mean flow cannot be directly estimated from observations without orders of magnitude uncertainty (Alexander and Sato 2015).

Without a direct way of measuring key quantities in GW drag parameterizations (i.e: momentum flux as a function of wave direction and phase speed at the source level) globally, tuning parameters are estimated indirectly. The free parameters are chosen to be physically reasonable and then the mean wind and temperature of the middle atmosphere, which are relatively well observed, provide an indirect verification measure for gravity wave parameterizations. In other words, during the development of new versions of GCMs, gravity wave parameterizations are 'tuned' in order to arrive at a reasonable representation of the observed zonal-mean climate. Such an exercise assumes errors from other parts of the model (e.g. the dynamical core, other parameterizations) are small, that the form of the GW drag parameterizations are correct, and that errors that remain are attributable to the GW drag parameterizations and ultimately incorrectly specified tuning parameters. These tuning parameters are adjusted in order to best represent the observed mean climate. These assumptions are, of course, not valid; however, such an exercise is common practice in developing climate models. Tuning of GW drag parameterizations likely results in the GW parameterizations compensating for other model errors (e.g. horizontal and vertical discretization errors, numerical diffusion, errors in other parameterizations, errors in GW parameterization structure).

Gravity wave tuning is an iterative process which consists of changing the unconstrained parameterization parameters, running the climate model, and assessing model climatology and biases. The process is repeated typically several to several dozen times until an acceptable modeled climate state is achieved. Models with fixed GW sources typically have one set of tunable parameters and with those they need to arrive at reasonable tropical and extratropical mean wind and temperature in the stratosphere, and also in the mesosphere (if the model extends this high). Despite many GW tuning efforts, many GCMs end up with a 'cold-pole bias' in the Southern Hemisphere winter polar stratosphere (e.g: Eyring et al. (2006), Austin et al. (2003)) which can be improved by additional GW drag in the southern hemisphere (Garcia et al. 2017). In addition, many recent climate models have internally generated QBOs which are largely driven by parameterized gravity waves (e.g.: Giorgetta et al. 2006, Richter et al. 2014 and Geller et al. 2016) and hence GW parameterization parameters must be just right to get a reasonable period of the QBO close to observed in addition to the mean wind and temperature in the middle atmosphere. Source oriented GW parameterizations allow more flexibility while tuning GWs, as typically in models such as WACCM (Richter et al. 2010) and LMDz (Lott et al. 2012, Lott and Guez 2013), convectively generated GWs control the Tropics: QBO and SAO, whereas the orographic and frontal waves affect the extratropical mean state. More complexity and options in GW parameterization parameters, however also means endless combinations of poorly constrained parameters, which is also difficult to deal with.

11.2.5 Missing processes

Again, GWs are treated as linear, hydrostatic, only propagating vertically (in a slowly-varying background in z, no less), propagating upward instantaneously, and propagating through a steady ambient environment with Boussinesq governing equations. All these simplifications lurking in the underlying physics prevent representation of many GW characteristics that are well observed and physically understood.

For example, non-orographic GW observations show strong amplitude intermittency, where infrequently observed waves with very large amplitudes can represent very high fractions of time-averaged momentum flux. Indeed, from observations in the lower stratosphere (Hertzog et al. 2012), distributions of individual event wave momentum fluxes have shown a log-normal distribution of amplitudes, with the largest amplitude waves occurring <10% of the time but carrying ~60% of the average flux. Such amplitude intermittency is generally not well represented, or not represented at all, having important implications for the total momentum fluxed and levels where it gets deposited. GW parameterizations that have GW sources tied to particular mechanisms (e.g. convective parameterizations, frontogenesis metrics, MW parameterizations, see following sections) do have some representation of intermittency, tied to the intermittency of the sources represented by the host model. Still, the infrequent, but very large-amplitude GWs remain underrepresented (e.g. Stephan et al. (2016)).

Stochasticity in parameterized gravity wave sources is another way to account for wave intermittency. Eckermann (2011) demonstrated that stochastic representation of the non-orographic wave spectrum in different grid points gave similar middle atmospheric circulation changes as including the full spectrum uniformly, but at much lower computational cost. These ideas have found use in modern parameterization schemes (de la Camara et al. 2014, Serva et al. 2018) with some demonstrated improvements in model performance.

Numerous other characteristics of GWs are unrepresented as a result of the many conventional, and sometimes pragmatic, assumptions and simplifications made. Non-hydrostatic influences occur when the GW intrinsic frequency becomes close to the buoyancy frequency and can reduce orographic drag (e.g. Smith and Kruse 2017) and result in wave reflection and trapping, which can also influence drag (see Section 8 of Tiexeira 2014 for an overview). Neglecting lateral-propagation results in significant overestimates of MW amplitudes, breaking and drag at altitudes that are too low, and drag that is too spatially confined (e.g. Eckermann et al. 2015b). Trailing MWs launched terrain orientations oblique to the source-level flow can propagate horizontally for O(1000) kilometers (e.g. Sato et al. 2012, Amemiya and Sato 2016, Jiang et al. 2019), and neglect of such long-distance propagation is likely in part responsible for an artificial gap in GW drag near 60S in climate models that significantly influences Southern Hemisphere polar night jet strength (McLandress et al. 2012, Kruse et al. 2021).

Transience of both the GWs and their background can also be important. Transient forcing results in vertical dispersion and spreading of GWs due to the spectrum of vertical group velocities of the generated spectrum of GWs (e.g. Chen et al. 2007, Kruse and Smith 2018), which influence wave amplitudes and breaking levels. Increasing and decreasing flow over terrain result in MWs with positive and negative phase speeds and propagation downstream and upstream of the mountains, respectively. Transient forcing also induces transient wave packet propagation, allowing interaction of the GW packet with the environment it propagates into and out of even without breaking (Fritts and Dunkerton 1984, Bühler and McIntyre 1999, 2003, 2005, Dosser and Sutherland 2011, Bölöni et al. 2016, Kruse and Smith 2018). Ray tracing methods have been applied in research models to account for horizontal propagation and group velocity effects (Song and Chun 2008, Bölöni et al. 2016), but these have not found wider application because of computational costs.

To summarize, GWs are very important in Earth's atmosphere, and their representation in all weather and climate models that do not fully resolve the entire GW spectrum is essential. The various parameterizations implemented do improve weather and climate model skill. Still, there is much potential to improve parameterizations via both better observational constraints and improving the underlying physics.

Acknowledgements

CGK was supported by the National Science Foundation (NSF, grant #2004512) and in part by an Advanced Study Program fellowship at the National Center for Atmospheric Research, which is also supported by the NSF under Cooperative Agreement 1852977. JHR and JTB were supported by NCAR as well. MJA was supported by both the NSF (grant #1829373) and NASA (grant #80NSSC17K0169). The mountain wave simulation in Fig. 1 and Supplemental Animation 1 were performed using high-performance computing support from Cheyenne (doi:10.5065/D6RX99HX) provided by NCAR's Computational and Information Systems Laboratory, sponsored by the National Science Foundation. JW was supported by the National Natural Science Foundation of China (Grant 42075005) and Guangdong Province Key Laboratory for Climate Change and Natural Disaster Studies (Grant 2020B1212060025).

.

References

Alaka, M. A., 1960: *The Airflow Over Mountains.* WMO Technical Note No. 34. World Meteorological Organization, Geneva. 137pp.

Adachi, Y., Yukimoto, S., Deushi, M., Obata, A., Nakano, H., Tanaka, T. Y., Hosaka, M., Sakami, T., Yoshimura, H., Hirabara, M., Shindo, E., Tsujino, H., Mizuta, R., Yabu, S., Koshiro, T., Ose, T., and Kitoh, A.: Basic performance of a new earth system model of the Meteorological Research Institute (MRI-ESM1), Papers in Meteor. and Geophys., 64, 1–19, 2013.

Alexander, M. J., and T. J. Dunkerton, A spectral parameterization of mean-flow forcing due to breaking gravity waves,*J. Atmos. Sci.*, *56*, 4167–4182, 1999.

Alexander, M. J, J. R. Holton, and D. R. Durran, 1995: The gravity wave response above deep convection in a squall line simulation. *J. Atmos. Sci.,* **52,**2212–2226.

Alexander M. J, and J. Holton, 1997: A model study of zonal forcing in the equatorial stratosphere by convectively induced gravity waves.J. Atmos. Sci., 54, 408–419.

Alexander M. J. and J. R. Holton, 2004: On the spectrum of vertically propagating gravity waves generated by a transient heat source. Atmospheric Chemistry and Physics Discussions, European Geosciences Union, 2004, 4 (1), pp.1063-1090.

Alexander, M. J., and D. A. Ortland (2010), Equatorial waves in High Resolution Dynamics Limb Sounder (HIRDLS) data, *J. Geophys. Res.*,*115*, D24111, doi:10.1029/2010JD014782.

Alexander, M., and K. Rosenlof, Nonstationary gravity wave forcing of the stratospheric zonal mean wind, J. Geophys. Res., 101, 23,465–23,474, 1996.

Alexander, M. J., and K. H. Rosenlof (2003), Gravity wave forcing in the stratosphere: Observational constraints from UARS and implications for parameterization in global models, J. Geophys. Res., 108(D19), doi:10.1029/2003JD003,373.

Alexander, M. J., and Coauthors, 2008: Global estimates of gravity wave momentum flux from High Resolution Dynamics Limb Sounder observations. J. Geophys. Res., 113, D15S18, doi:10.1029/ 2007JD008807.

Alexander, M. J., and T. J. Dunkerton, 1999: A spectral parameterization of mean-flow forcing due to breaking gravity waves, *J. Atmos. Sci.*, *56*, 4167–4182

Alexander, M. J., Eckermann, S. D., Broutman, D., and Ma, J. (2009), Momentum flux estimates for South Georgia Island mountain waves in the stratosphere observed via satellite, *Geophys. Res. Lett.*, 36, L12816, doi:10.1029/2009GL038587.

Alexander, M. J. and K. Sato, SPARC Newsletter No. 44, 2015, p. 9: Gravity Wave Dynamics and Climate: An Update from the SPARC Gravity Wave Activity

Amemiya, A and K. Sato, 2016: A new gravity wave parameterization including three-dimensional propagation. J. Meteorological Soc. of Japan, Vol. 94, No. 3, pp. 237-256. DOI:10.2151/jmsj.2016-013

Austin, J., et al. (2003), Uncertainties and assessments of chemistry-climate models of the stratosphere, Atmos. Chem. Phys., 3, 1–27.

Azeem, I., S. L. Vadas, G. Crowley, and J. J. Makela, 2017, Traveling ionospheric disturbances over the United States induced by gravity waves from the 2011 Tohoku tsunami and comparison with gravity wave dissipative theory, J. Geophys. Res. Space Physics, 122, 3430–3447, doi:10.1002/2016JA023659.

Bacmeister, J.T. and R.T. Pierrehumbert, 1988: On High-Drag States of Nonlinear Stratified Flow over an Obstacle. *J. Atmos. Sci.,* **45**, 63–80, https://doi.org/10.1175/1520-0469(1988)045<0063:OHDSON>2.0.CO;2

Bacmeister, J. T., and M. R. Schoeberl, 1989: Breakdown of vertically propagating two-dimensional gravity waves forced by orography. *J. Atmos. Sci.,* **46,** 2109–2134.

Bacmeister, J. T., Mountain-wave drag in the stratosphere and mesosphere inferred from observed winds and a simple mountain-wave parameterization scheme, J. Atmos. Sci., 50, 377–399, 1993.

Baines, P. G, and T. N. Palmer, Rationale for a new physically-based parameterisation of sub-grid scale orographic effects., Tech. Rep. 169, ECMWF (1990)

Bakas, N., and B. Farrell (2008), Momentum and energy transport by gravity waves in stochastically driven stratified flows. Part II: Radiation of gravity waves from a Gaussian jet, *J. Atmos. Sci.*, *65*(7), 2308–2325.

Bakas, N., and B. Farrell (2009a), Gravity waves in a horizontal shear flow. Part I: Growth mechanisms in the absence of potential vorticity perturbations., *J. Phys. Oceanogr.*, *39*, 481–496.

Bakas, N., and B. Farrell (2009b), Gravity waves in a horizontal shear flow. Part II: Interaction between gravity waves and potential vorticity perturbations, *J. Phys. Oceanogr.*, *39*, 497–511.

Baldwin, M. P., et al. (2001), The quasi-biennial oscillation, Rev. Geophys., 39, 179–229.

Beljaars, A. C. M., Brown, A. R. and Wood, N. (2004), A new parametrization of turbulent orographic form drag. Q.J.R. Meteorol. Soc., 130: 1327–1347. doi:10.1256/qj.03.73.

Beres, J. H., M. J. Alexander, and J. R. Holton, 2002: Effects of tropospheric wind shear on the spectrum of convectively generated gravity waves. *J. Atmos. Sci.,* **59,** 1805–1824.

Beres, J. H., M. J. Alexander, and J. R. Holton, 2004: A method of specifying the gravity wave spectrum above convection based on latent heating properties and background wind. *J. Atmos. Sci*, **61,** 324–337.

Beres J. H., 2004: Gravity Wave Generation by a Three-Dimensional Thermal Forcing. *Journal of the Atmospheric Sciences* **61**:14, 1805-1815.

Beres, J. H., R. R. Garcia, B. A. Boville, and F. Sassi (2005), Implementation of a gravity wave source spectrum parameterization dependent on the properties of convection in the Whole Atmosphere Community Climate Model (WACCM), J. Geophys. Res., 110, D10108, doi:10.1029/2004JD005504.

Boer, G. J., N. A. McFarlane, R. Laprise, J. D. Henderson and J.-P. Blanchet. 1984. The Canadian Climate Centre spectral atmospheric general circulation model. Atmosphere-Ocean, **22**: 397–429.

Bossert K., C. Kruse, C. Heale, D. C. Fritts, J. Snively P.-D. Pautet, B. P. Williams, M. J. Taylor (2017), Secondary Gravity Wave Generation Over New Zealand During the DEEPWAVE Campaign, *J. Geophys. Res. Atmos.,* doi:10.1002/2016JD026079.

Bossert, K., Fritts, D. C., Heale, C. J., Eckermann, S. D., Plane, J. M. C., Snively, J. B., et al. (2018). Momentum flux spectra of a mountain wave event over New Zealand. *Journal of Geophysical Research: Atmospheres*, 123, 9980–9991. https://doi-org.cuucar.idm.oclc.org/10.1029/2018JD028319

Bölöni, G., B. Ribstein, J. Muraschko, C. Sgoff, J. Wei, and U. Achatz, 2016: The interaction between atmospheric gravity waves and large-scale flows: An efficient description beyond the nonacceleration paradigm. J. Atmos. Sci., 73, 4833–4852, doi:10.1175/JAS-D-16-0069.1.

Boville, B. 1986. Wave-mean flow interactions in a general circulation model of the troposphere and stratosphere. *J. Atmos. Sci.* **43**: 1711–1725.

Boville, B. A. (1991), Sensitivity of simulated climate to model resolution, J. Climate, 4, 469–485.

Bretherton, C.: Group velocity and the linear response of stratified fluids to internal heat or mass sources, J.Atmos.Sci.,45,81–93,1988.

Bretherton, C. S., and P. K. Smolarkiewicz, 1989: Gravity waves, compensating subsidence and detrainment around cumulus clouds. J. Atmos. Sci, **46,** 740–759.
Bramberger, M., Dörnbrack, A., Bossert, K., Ehard, B., Kaifler, B., Mallaun, C., … Witschas, B. (2017). Does Strong tropospheric forcing cause large-amplitude mesospheric gravity waves? A DEEPWAVE case study. *Journal of Geophysical Research: Atmospheres*, 122, 11,422–11,443. https://doi.org/10.1002/2017JD027371

Broutman, D., S. D. Eckermann, H. Knight, and J. Ma (2017), A stationary phase solution for mountain waves with application to mesospheric mountain waves generated by Auckland Island, *J. Geophys. Res. Atmos.*, 122, 699–711, doi:10.1002/2016JD025699.

Bühler, O., and M. E. McIntyre, 1999: On shear-generated gravity waves that reach the mesosphere. part II: Wave propagation. J. Atmos. Sci., 56, 3764–3773.

Bühler, O., and M. E. McIntyre, 2003: Remote recoil: a new wave-mean interaction effect. J. Fluid Mech., 492, 207–230.

Bühler, O., and M. E. McIntyre, 2005: Wave capture and wave-vortex duality. J. Fluid Mech., 534, 67–95, doi:10.1017/S0022112005004374.

Bühler, O., M. McIntyre, and J. Scinocca (1999), On shear-generated gravity waves that reach the mesosphere. Part I: Wave generation, *J. Atmos. Sci.*, *56*, 3749–3763.

Burleigh, M. R., Heale, C. J., Zettergren, M. D., & Snively, J. B. (2018). Modulation of low-altitude ionospheric upflow by linear and nonlinear atmospheric gravity waves. *Journal of Geophysical Research: Space Physics*, 123. https://doi.org/10.1029/2018JA025721

Bushell, A. C., Butchart, N., Derbyshire, S. H., Jackson, D. R., Shutts, G. J., Vosper, S. B., & Webster, S. (2015). Parameterized gravity wave momentum fluxes from sources related to convection and large-scale precipitation processes in a global atmosphere model. *Journal of the Atmospheric Sciences*, *72*(11), 4349–4371.

Bushell, AC, Anstey, JA, Butchart, N, et al. Evaluation of the Quasi-Biennial Oscillation in global climate models for the SPARC QBO-initiative. *QJR Meteorol Soc*. 2020; 1– 31. https://doi.org/10.1002/qj.3765

Butchart, N., and J. Austin, Middle atmosphere climatologies from the troposphere-stratosphere configuration of the ukmo's unified model, J. Atmos. Sci., 55, 2782–2809, 1998.

Butchart, N., Anstey, J., Hamilton, K., Osprey, S., McLandress, C., Bushell, A., Kawatani, Y., Kim, Y.-H., Lott, F., Scinocca, J., Stock- dale, T., Andrews, M., Bellprat, O., Braesicke, P., Cagnazzo, C., Chen, C.-C., Chun, H.-Y., Dobrynin, M., Garcia, R., Garcia- Serrano, J., Gray, L., Holt, L., Kerzenmacher, T., Naoe, H., Pohlmann, H., Richter, J., Scaife, A., Schenzinger, V., Serva, F., Versick, S., Watanabe, S., Yoshida, K. and Yukimoto, S. (2018) Overview of experiment design and comparison of models participating in phase 1 of the SPARC Quasi-Biennial Oscillation initiative (QBOi). *Geoscientific Model Development*, **11**, 1009–1032.

de la Cámara A., F. Lott and A. Hertzog, Intermittency in a stochastic parameterization of nonorographic gravity waves, *Journal of Geophysical Research: Atmospheres*, 119, 21, (11,905-11,919), (2014).

Cámara, A. and F. Lott, A parameterization of gravity waves emitted by fronts and jets,*Geophysical Research Letters*, 42, 6, (2071-2078), (2015).

Cámara, A. d. l., Lott, F., Jewtoukoff, V., Plougonven, R., & Hertzog, A. (2016). On the Gravity Wave Forcing during the Southern Stratospheric Final Warming in LMDZ, *Journal of the Atmospheric Science*s, 73(8), 3213-3226.

Charron, M. and E. Manzini, 2002: Gravity Waves from Fronts: Parameterization and Middle Atmosphere Response in a General Circulation Model. J. Atmos. Sci., **59**,923–941, https://doi.org/10.1175/1520-0469(2002)059<0923:GWFFPA>2.0.CO;2

Chen, C.-C., D. R. Durran, and G. J. Hakim, 2005: Mountain-wave momentum flux in an evolving synoptic-scale flow. J. Atmos. Sci., 62, 3213–3231, https://doi.org/10.1175/JAS3543.1.

Chen, C., Hakim, G. J., & Durran, D. R. (2007). Transient Mountain Waves and Their Interaction with Large Scales, *Journal of the Atmospheric Sciences*, *64*(7), 2378-2400.

Chimonas, G., and J. Grant (1984), Shear excitation of gravity waves. Part II: Upscale scattering from Kelvin-Helmholtz waves, *J. Atmos. Sci.*, *41*, 2278–2288.

H. -J. Choi and H. -Y. Chun. (2013) Effects of Convective Gravity Wave Drag in the Southern Hemisphere Winter Stratosphere. *Journal of the Atmospheric Sciences* 70:7, 2120-2136.

Chun, H.-Y., and J.-J. Baik, 1998: Momentum flux by thermally induced internal gravity waves and its approximation for large-scale models. *J. Atmos. Sci.,* **55,** 3299–3310.

Chun, H-Y., M-D. Song, J-W. Kim, and J-J. Baik, 2001a: Effects of gravity wave drag induced by cumulus convection on the atmospheric general circulation. *J. Atmos. Sci*, **58,** 302–319.

Chun, H.-Y., and J.-J. Baik, 2002: An updated parameterization of convectively forced gravity wave drag for use in large-scale models. *J. Atmos. Sci.,* **59,** 1006–1017.

Chun, H.-Y., I.-S. Song, J.-J Baik, and Y-J. Kim, (2004) Impact of a Convectively Forced Gravity Wave Drag Parameterization in NCAR CCM3. *Journal of Climate* **17**:18, 3530-3547.

Chun, H.-Y., J.-J..Baik, and T. Horinouchi, 2005: Momentum flux spectrum of convectively forced gravity waves: Can diabatic forcing be a proxy for convective forcing? J. Atmos. Sci., **62**, 4113–4120

Chun, H.-Y., and Y.-H. Kim(2008), Secondary waves generated by breaking of convective gravity waves in the mesosphere and their influence in the wave momentum flux, J. Geophys. Res., 113, D23107, doi:10.1029/2008JD009792

Chun, H.-Y., H.-J. Choi, and I.-S. Song, 2008: Effects of nonlinearity on convectively forced internal gravity waves: Application to a gravity wave drag parameterization. *J. Atmos. Sci.*, **65**, 557–575, doi:https://doi.org/10.1175/2007JAS2255.1.

Choi H-J. and H-Y. Chun. (2011) Momentum Flux Spectrum of Convective Gravity Waves. Part I: An Update of a Parameterization Using Mesoscale Simulations. *Journal of the Atmospheric Sciences* 68:4, 739-759.

Clark, T.L. and W.R. Peltier, 1977: On the Evolution and Stability of Finite-Amplitude Mountain Waves. *J. Atmos. Sci.,* **34**, 1715–1730, https://doi.org/10.1175/1520-0469(1977)034<1715:OTEASO>2.0.CO;2

Clark, T.L. and W.R. Peltier, 1984: Critical Level Reflection and the Resonant Growth of Nonlinear Mountain Waves. *J. Atmos. Sci.,* **41**, 3122–3134,https://doi.org/10.1175/1520-0469(1984)041<3122:CLRATR>2.0.CO;2

Clark, T. L., T. Hauf, and J. P. Kuettner, 1986: Convectively forced internal gravity waves: Results from two-dimensional numerical experiments. Quart. J. Roy. Meteor. Soc.,**112,** 899–925

Choi H.-J. and H-Y. Chun. (2011) Momentum Flux Spectrum of Convective Gravity Waves. Part I: An Update of a Parameterization Using Mesoscale Simulations. Journal of the Atmospheric Sciences **68**:4, 739-759.

Davini, P., von Hardenberg, J., Corti, S., Christiansen, H. M., Juricke, S., Subramanian, A., Watson, P. A. G., Weisheimer, A., and Palmer T. N.: Climate SPHINX: evaluating the impact of resolution and stochastic physics parameterisations in the EC-EARTH global climate model, Geosci. Model Dev. 10, 1383–1402, doi:10.5194/gmd-10-1383-2017, 2017.

Dörnbrack, A., M. Leutbecher, R. Kivi, and E. Kyrö, Mountain- wave induced record low stratospheric temperatures above northern Scandinavia, *Tellus, Ser. A*, *51*, 951–963, 1999.

Dosser, H. V., and B. R. Sutherland, 2011: Anelastic internal wave packet evolution and stability. J. Atmos. Sci., 68, 2844–2859, doi:10.1175/JAS-D-11-097.1.

Drazin P. G. (1961) On the steady flow of a fluid of variable density past an obstacle. Tellus 13:239–251

Dunkerton, T. J. (1982), Theory of the mesopause semiannual oscillation, J. Atmos. Sci., 39, 2681–2690.

Dunkerton, T. J. (1997), The role of gravity waves in the quasi-biennial oscillation, J. Geophys. Res., 102(D22), 26,053–26,076.

Durran, D.R. and J.B. Klemp, 1983: A Compressible Model for the Simulation of Moist Mountain Waves. *Mon. Wea. Rev.,* **111**, 2341–2361, https://doi.org/10.1175/1520-0493(1983)111<2341:ACMFTS>2.0.CO;2

Durran, D.R., 1986: Mountain Waves (Mesoscale Meteorology and Forecasting). American Meteorological Society, Boston, pp 472-492.

Durran, D.R., 1986a: Another look at downslope windstorms. Part I: On the development of analogs to supercritical flow in an infinitely deep continuously stratified fluid. J. Atmos. Sci., 93, 2527-2543.

Durran, D.R., 1986b: Mountain Waves (Mesoscale Meteorology and Forecasting). American Meteorological Society, Boston, pp 472-492.

Durran, D.R. and J.B. Klemp, 1987: Another Look at Downslope Winds. Part II: Nonlinear Amplification beneath Wave-Overturning Layers. *J. Atmos. Sci.,* **44**, 3402–3412,https://doi.org/10.1175/1520-0469(1987)044<3402:ALADWP>2.0.CO;2

Durran, D.R. 1990. Mountain waves and downslope winds. In: Atmospheric Processes over Complex Terrain. W. Blumen, (Ed), Meteorol. Monogr. Am. Meteorol. Soc. 23 (45): 59–81.

Durran, D. R. 2003. Lee waves and mountain waves. Encyclopedia of Atmospheric Sciences (eds.J. R.Holton, J. Pyle and J. A. Curry). Elsevier Science Ltd., London, 1161-1170.

Eckermann, S. D. (2011), Explicitly stochastic parameterization of nonorographic gravity wave drag, J. Atmos. Sci., 68, 1749–1765.

Eckermann, S. D., J. Ma, and D. Broutman, 2015: Effects of horizontal geometrical spreading on the parameterization of orographic gravity wave drag. Part I: Numerical transform solutions. J. Atmos. Sci., 72, 2330–2347, https://doi.org/10.1175/JAS-D-14-0147.1.

Eckermann, S. D., Broutman, D., & Knight, H. (2015). Effects of Horizontal Geometrical Spreading on the Parameterization of Orographic Gravity Wave Drag. Part II: Analytical

Solutions, *Journal of the Atmospheric Sciences*, *72*(6), 2348-2365. Retrieved Oct 7, 2021, from https://journals.ametsoc.org/view/journals/atsc/72/6/jas-d-14-0148.1.xml

Eckermann, S.D., D. Broutman, J. Ma, J.D. Doyle, P. Pautet, M.J. Taylor, K. Bossert, B.P. Williams, D.C. Fritts, and R.B. Smith, 2016: Dynamics of Orographic Gravity Waves Observed in the Mesosphere over the Auckland Islands during the Deep Propagating Gravity Wave Experiment (DEEPWAVE). *J. Atmos. Sci.,* **73**, 3855–3876,https://doi.org/10.1175/JAS-D-16-0059.1

Eliassen, A., and E. Palm, 1960: On the transfer of energy in stationary mountain waves. Geofys. Publ., 22 (3), 1–23.

Ern, M., P. Preusse, M. J. Alexander, and C. D. Warner, 2004: Absolute values of gravity wave momentum flux derived from satellite data. J. Geophys. Res., 109, D20103, doi:10.1029/2004JD004752.

Ern, M., L. Hoffmann, and P. Preusse, 2017: Directional gravity wave momentum fluxes in the stratosphere derived from high-resolution AIRS temperature data. *Geophys. Res. Lett.*, **44 (1)**, 475–485, https://doi.org/10.1002/2016GL072007.

Eyring, V., and Coauthors, 2006: Assessment of temperature, trace spices, and ozone in chemistry-climate model simulations of the recent past. J. Geophys. Res., **111,** D22308. doi:10.1029/2006JD007327.

Eyring, V., et al. (2007), Multimodel projections of stratospheric ozone in the 21st Century, J. Geophys. Res., 112(D16303), doi:10.1029/2006JD008,332.

Farmer, D. M. & Armi, L. (1999): The generation and trapping of solitary waves over topography. *Science* **283**, 188–190

Felten, F. N., and T. S. Lund (2006), Kinetic energy conservation issues associated with the collocated mesh scheme for incompressible flow, *J. Comput. Phys.*, 215, 465–484.

Ford, R., M. E. McIntyre, and W. A. Norton (2000), Balance and the slow quasi manifold: Some explicit results, *J. Atmos. Sci.*, *57*, 1236–1254.

Ford, R., 1994a: Gravity wave radiation from vortex trains in rotating shallow water, J. Fluid Mech., 281, 81–118.

Ford, R., 1994b: The response of a rotating ellipse of uniform potential vorticity to gravity wave radiation, Phys. Fluids, 6(11), 3694–3704.

Fovell, R., D. Durran, and J. R. Holton, 1992: Numerical simulations of convectively generated stratospheric gravity waves. J. Atmos. Sci.,**49,** 1427–1442

Fovell, R. G., Mullendore, G. L., & Kim, S. (2006). Discrete Propagation in Numerically Simulated Nocturnal Squall Lines, *Monthly Weather Review*, 134(12), 3735-3752.

Franke, P. M., and W. A. Robinson(1999),Nonlinear behavior in the propagation of atmospheric gravity waves, J. Atmos. Sci.,56, 3010–3027.

Fritts, D. C., and Z. Luo (1992), Gravity wave excitation by geostrophic adjustment of the jet stream. Part I: Two-dimensional forcing, *J. Atmos. Sci.*, *49*(8), 681–697.

Fritts, D. C., & Dunkerton, T. J. (1984). A Quasi-Linear Study of Gravity-Wave Saturation and Self-Acceleration, *Journal of Atmospheric Sciences*, *41*(22), 3272-3289.

Fritts, D. (1984), Shear excitation of atmospheric gravity waves. 2: Nonlinear radiation from a free shear layer, *J. Atmos. Sci.*, *41*, 524–537.

Fritts, D. C., and W. Lu, Spectral estimates of gravity wave energy and momentum fluxes, II, Parameterization of wave forcing and variability, *J. Atmos. Sci.*, *50*, 3695–3713, 1993.

Fritts, D. C., and Alexander, M. J. (2003), Gravity wave dynamics and effects in the middle atmosphere, *Rev. Geophys.*, 41, 1003, doi:10.1029/2001RG000106, 1.

Fritts, D.C., R.B. Smith, M.J. Taylor, J.D. Doyle, S.D. Eckermann, A. Dörnbrack, M. Rapp, B.P. Williams, P. Pautet, K. Bossert, N.R. Criddle, C.A. Reynolds, P.A. Reinecke, M. Uddstrom, M.J. Revell, R. Turner, B. Kaifler, J.S. Wagner, T. Mixa, C.G. Kruse, A.D. Nugent, C.D. Watson, S. Gisinger, S.M. Smith, R.S. Lieberman, B. Laughman, J.J. Moore, W.O. Brown, J.A. Haggerty, A. Rockwell, G.J. Stossmeister, S.F. Williams, G. Hernandez, D.J. Murphy, A.R. Klekociuk, I.M. Reid, and J. Ma, 2016: The Deep Propagating Gravity Wave Experiment (DEEPWAVE): An Airborne and Ground-Based Exploration of Gravity Wave Propagation and Effects from Their Sources throughout the Lower and Middle Atmosphere. *Bull. Amer. Meteor. Soc.,* **97**, 425–453, https://doi.org/10.1175/BAMS-D-14-00269.1

Fritts, D. C., Vosper, S. B., Williams, B. P., Bossert, K., Plane, J. M. C., Taylor, M. J., et al. (2018). Large-amplitude mountain waves in the mesosphere accompanying weak cross-mountain flow during DEEPWAVE Research Flight RF22. *Journal of Geophysical Research: Atmospheres*, 123, 9992–10,022. https://doi.org/10.1029/2017JD028250

Garcia, R.R. and J.H. Richter, 2019: On the Momentum Budget of the Quasi-Biennial Oscillation in the Whole Atmosphere Community Climate Model. J. Atmos. Sci., **76**,69–87, https://doi.org/10.1175/JAS-D-18-0088.1

Garcia, R. R., and B. A. Boville (1994), “Downward control” of the mean meridional circulation and temperature distribution of the polar winter stratosphere, J. Atmos. Sci., 51, 2238–2245.

Garcia, R. R., and S. Solomon, The effect of breaking gravity waves on the dynamics and chemical composition of the mesosphere and lower thermosphere, *J. Geophys. Res.*, *90*, 3850–3868, 1985.

Garcia R. G. , A. K. Smith, D. E. Kinnison, Á. de la Cámara, and D. J. Murphy, 2017: Modification of the gravity wave parameterization in the Whole Atmosphere Community Climate Model: Motivation and results. J. Atmos. Sci., 74, 275–291, doi:10.1175/JAS-D-16-0104.1.

Garfinkel, C. I., & Oman, L. D. (2018). Effect of gravity waves from small islands in the Southern Ocean on the Southern Hemisphere atmospheric circulation. *Journal of Geophysical Research: Atmospheres*, 123, 1552–1561, https://doi.org/10.1002/2017JD027576.

Garner, S. T., 2005: A topographic drag closure built on an ana- lytical base flux. J. Atmos. Sci., 62, 2302–2315, https://doi.org/ 10.1175/JAS3496.1.

Geller, M.A., M.J. Alexander, P.T. Love, J. Bacmeister, M. Ern, A. Hertzog, E. Manzini, P. Preusse, K. Sato, A.A. Scaife, and T. Zhou, 2013: A Comparison between Gravity Wave Momentum Fluxes in Observations and Climate Models. J. Climate, **26**, 6383–6405, https://doi.org/10.1175/JCLI-D-12-00545.1

Geller, M.A., T.H. Zhou, D. Shindell, R. Ruedy, I. Aleinov, L. Nazarenko, N. Tausnev, M. Kelley, S. Sun, Y. Cheng, R.D. Field, and G. Faluvegi, 2016: Modeling the QBO — Improvements resulting from higher model vertical resolution. J. Adv. Model. Earth Syst., **8**, no. 3, 1092-1105, doi:10.1002/2016MS000699.

Gettelman, A., Mills, M. J., Kinnison, D. E., Garcia, R. R., Smith, A. K., Marsh, D. R., et al. (2019). The whole atmosphere community climate model version 6 (WACCM6). *Journal of Geophysical Research: Atmospheres*, 124, 12380– 12403. https://doi.org/10.1029/2019JD030943

Giorgetta, M. A., L. Bengtsson, and K. Arpe (1999), An investigation of QBO signals in the east Asian and Indian monsoon in GCM experiments,Clim. Dyn., 15(6), 435–450, doi:10.1007/s003820050292.

Giorgetta, M. A., E. Manzini, E. Roeckner, M. Esch, and L. Bengtsson (2006), Climatology and forcing of the quasi-biennial oscillation in the MACHAM5 model, *J. Clim.*, *19*, 3882–3901.

Gossard, E.E., and William H. Hooke, 1975: Waves in the Atmosphere. Elsevier, New York, 456pp.

Guest, F.M., M.J. Reeder, C.J. Marks, and D.J. Karoly. 2000. Inertia-gravity waves observed in the lower stratosphere over Macquarie Island. *J. Atmos. Sci*. **57**: 737–752.

Heale, C. J., Snively, J. B., Hickey, M. P., & Ali, C. J. (2014). Thermospheric dissipation of upward propagating gravity wave packets. *Journal of Geophysical Research: Space Physics*, *119*, 3,857–3,872. https://doi.org/10.1002/2013JA019387

Heale, C. J., and J. B. Snively (2015), Gravity wave propagation through a vertically and horizontally inhomogeneous background wind, *J. Geophys. Res. Atmos.*, *120*, 5931–5950, doi:10.1002/2015JD023505.

Heale, C. J., K. Bossert, J. B. Snively, D. C. Fritts, P.-D. Pautet, and M. J. Taylor (2017), Numerical modeling of a multiscale gravity wave event and its airglow signatures over Mount Cook, New Zealand, during the DEEPWAVE campaign, *J. Geophys. Res. Atmos.*, 122, 846–860, doi: 10.1002/2016JD025700.

Heale, C. J., Walterscheid, R. L., & Snively, J. B. (2018). Localization effects on the dissipation of gravity wave packets in the upper mesosphere and lower thermosphere. *Journal of Geophysical Research: Atmospheres*, 123, 8915– 8935. https://doi.org/10.1029/2017JD027617

Heale, C. J., Lund, T., & Fritts, D. C. (2020). Convectively generated gravity waves during solstice and equinox conditions. *Journal of Geophysical Research: Atmospheres*, 125, e2019JD031582. https://doi.org/10.1029/2019JD031582

Hertzog, A.,, G. Boccara, R. A. Vincent, F. Vial, and P. Cocquerez, 2008: Estimation of gravity-wave momentum fluxes and phase speeds from quasi-Lagrangian stratospheric balloon flights. 2: Results from the Vorcore campaign in Antarctica. J. Atmos. Sci., 65, 3056–3070.

Hindley, N. P., C. J. Wright, L. Hoffmann, T. Moffat-Griffin, and N. J. Mitchell, 2020: An 18-year climatology of directional stratospheric gravity wave momentum flux from 3-d satellite obser- vations. *Geophys. Res. Lett.*, **47 (22)**, https://doi.org/https://doi.org/10.1029/2020GL089557.

Hitchman, M. H., and C. B. Leovy (1988), Estimation of the Kelvin wave contribution to the semiannual oscillation, J. Atmos. Sci., 45, 1462 – 1475.

Hickey, M. P., R. L. Walterscheid, and G. Schubert (2011), Gravity wave heating and cooling of the thermosphere: Sensible heat flux and viscous flux of kinetic energy, J. Geophys. Res., 116, A12326, doi: https://doi.org/10.1029/2011JA016792

Hines, C. O. (1997a). Doppler-spread parameterization of gravity-wave momentum deposition in the middle atmosphere. Part 1: Basic formulation. *Journal of Atmospheric and Solar-Terrestrial Physics*, 59(4), 371–386. https://doi.org/10.1016/S1364-6826(96)00079-X

Hines, C. O. (1997b). Doppler-spread parameterization of gravity-wave momentum deposition in the middle atmosphere. Part 2: Broad and quasi monochromatic spectra, and implementation. *Journal of Atmospheric and Solar-Terrestrial Physics*, 59(4), 387–400.

Hoffmann, L., Xue, X., and Alexander, M. J. (2013), A global view of stratospheric gravity wave hotspots located with Atmospheric Infrared Sounder observations, *J. Geophys. Res. Atmos.*, 118, 416– 434, doi:10.1029/2012JD018658.

Hoffmann, L., Grimsdell, A. W., and Alexander, M. J.: Stratospheric gravity waves at Southern Hemisphere orographic hotspots: 2003–2014 AIRS/Aqua observations, Atmos. Chem. Phys., 16, 9381–9397, https://doi.org/10.5194/acp-16-9381-2016, 2016.

Holt, L. A., M. J. Alexander, M. J., L. Coy, C. Liu, A. Molod, W. Putman, and S. Pawson, 2017: An evaluation of gravity waves and their sources in the Southern Hemisphere in a 7-km global climate simulation, Q. J. Meteorol. Soc., 143(707), 2481–2495, doi:10.1002/qj.3101.

Holton, J. R., 1982, The role of gravity wave induced drag and diffusion in the momentum budget of the mesosphere, *J. Atmos. Sci.*, *39*, 791–799.

Holton, J. R., The influence of gravity wave breaking on the general circulation of the middle atmosphere, *J. Atmos. Sci.*,*40*, 2497–2507, 1983.

Holton, J. R., and M. J.Alexander, 1999: Gravity waves in the mesosphere generated by tropospheric convection.Tellus, 51A-B, 45–58.

Holton, J. R., J. H. Beres, and X. Zhou, 2002: On the vertical scale of gravity waves excited by localized thermal forcing. J. Atmos. Sci., **59**, 2019–2023, doi:https://doi.org/10.1175/1520-0469(2002)059<2019:OTVSOG>2.0.CO;2.

Holton, J. R., 2004: An Introduction to Dynamic Meteorology. 4th Edition. Volume 88 of International Geophysics Series. Elsevier Inc.

Hoskins, B. J., 1982: The mathematical theory of frontogenesis. *Annu. Rev. Fluid Mech.,* **14,** 131–151.

Hughes, M., A. Hall, and J. Kim, 2009: Anthropogenic reductions of Santa Ana winds. California Climate Change Center Rep. CEC-500-2009-015-D, 19 pp., www.energy.ca.gov/2009publications/CEC-500 -2009-015/CEC-500-2009-015-D.pdf.

Huppert, H., & Miles, J. (1969). Lee waves in a stratified flow Part 3. Semi-elliptical obstacle. *Journal of Fluid Mechanics, 35*(3), 481-496. doi:10.1017/S0022112069001236

Jiang, Q., J. D. Doyle, S. D. Eckermann, and B. P. Williams, 2019: Stratospheric trailing gravity waves from New Zealand. J. Atmos. Sci, in press.

Jewtoukoff, V., Plougonven, R., and Hertzog, A. (2013), Gravity waves generated by deep tropical convection: Estimates from balloon observations and mesoscale simulations, *J. Geophys. Res. Atmos.*, 118, 9690– 9707, doi:10.1002/jgrd.50781.

Jewtoukoff, V., A. Hertzog, R. Plougonven, A.d. Cámara, and F. Lott, 2015: Comparison of Gravity Waves in the Southern Hemisphere Derived from Balloon Observations and the ECMWF Analyses. J. Atmos. Sci., **72**, 3449–3468, https://doi.org/10.1175/JAS-D-14-0324.1

Jeon J., S-Y Hong, H-Y Chun, and I-S Song. (2010) Test of a convectively forced gravity wave drag parameterization in a general circulation model. *Asia-Pacific Journal of Atmospheric Sciences* **46**:1, 1-10.

Jiang Q., J. D. Doyle, S. Eckermann and B. P. Williams., 2019: Stratospheric Trailing Gravity Waves from New Zealand. JAS, under review.

Jin, Y. (1997), A numerical model study of the role of mesoscale gravity waves in rainband dynamics in the central United States during STORM-FEST, PhD dissertation, North Carolina State University.

Kaifler, B., N. Kaifler, B. Ehard, A. Dörnbrack, M. Rapp, and D. C. Fritts (2015), Influences of source conditions on mountain wave penetration into the stratosphere and mesosphere, *Geophys. Res. Lett.*, 42, 9488–9494, doi:10.1002/2015GL066465.

Kaplan, M., S. Koch, Y.-L. Lin, R. Weglarz, and R. Rozumalski (1997), Numerical Simulations of a Gravity Wave Event over CCOPE. Part I: The role of geostrophic adjustment in Mesoscale Jetlet Formation, *Mon. Weather Rev.*, *125*, 1185–1211.

Kawatani, Y., Watanabe, S., Sato, K., Dunkerton, T. J., Miyahara, S. and Takahashi, M. (2010) The Roles of Equatorial Trapped Waves and Internal Inertia–Gravity Waves in Driving the Quasi-Biennial Oscillation. Part II: Three-Dimensional Distribution of Wave Forcing. *Journal of the Atmospheric Sciences*, **67**, 981–997.

Kershaw, R., Parameterization of momentum transport by convectively generated gravity waves, *Q. J. R. Meteorol. Soc.*, *121*, 1023–1040, 1995.

Kim, Y. -J. and J. D. Doyle, 2005: Extension of an orographic-drag parameterization scheme to incorporate orographic anisotropy and flow blocking. Quart. J. Roy. Meteor. Soc., 131, 1893–1921,https://doi.org/10.1256/qj.04.160.

Klinker, E., & Sardeshmukh, P. D. (1992). The Diagnosis of Mechanical Dissipation in the Atmosphere from Large-Scale Balance Requirements, *Journal of Atmospheric Sciences*, *49*(7), 608-627. Retrieved Oct 8, 2021, from https://journals.ametsoc.org/view/journals/atsc/49/7/1520-0469_1992_049_0608_tdomdi_2_0_co_2.xml

2016 Kruse, C. G., R. B. Smith, and S. D. Eckermann: The Mid-Latitude Lower-Stratospheric Mountain Wave “Valve Layer”. Journal of the Atmospheric Sciences, 73, 5081-5100. doi:10.1175/JAS-D-16-0173.1.

Kruse, C.G. and R.B. Smith, 2018: Nondissipative and Dissipative Momentum Deposition by Mountain Wave Events in Sheared Environments. *J. Atmos. Sci.,* **75**, 2721–2740, https://doi.org/10.1175/JAS-D-17-0350.1

Kruse. C. G., M. J. Alexander, L. Hoffmann, A. van Niekerk, I. Polichtchouk, J. T. Bacmeister, L. Holt, R. Plougonven, P. Sacha, C. Wright, K. Sato, R. Shibuya, S. Gisinger, M. Ern, C. I. Meyer, and O. Stein, 2021: Observed and modeled mountain waves from the surface to the mesosphere near the Drake Passage. J. Atmos. Sci, Under review. JAS-D-21-0252.

Lac, C., J. P. Lafore, and J. L. Redelsperger, 2002: Role of gravity waves in triggering deep convection during TOGA COARE. J. Atmos. Sci., **59**, 1293–1316, doi:https://doi.org/10.1175/1520-0469(2002)059<1293:ROGWIT>2.0.CO;2.

Lane, T. P., and M. J. Reeder, 2001: Convectively generated gravity waves and their effect on the cloud environment. J. Atmos. Sci., 58, 2427–2440.

Lane, T. P., M. J. Reeder, and T. L. Clark, 2001: Numerical modeling of gravity wave generation by deep tropical convection. J. Atmos. Sci., **58**, 1249–1274, doi:https://doi.org/10.1175/1520-0469(2001)058<1249:NMOGWG>2.0.CO;2.

Lane, T. P., and R. D. Sharman(2006),Gravity wave breaking, secondary wave generation, and mixing above deep convection in a three-dimensional cloud model, Geophys. Res. Lett.,33, L23813, doi:10.1029/2006GL027988.

Lane T. P. , and F. Zhang, 2011: Coupling between gravity waves and tropical convection at mesoscales. J. Atmos. Sci., 68, 2582– 2598, doi:10.1175/2011JAS3577.1.

Leo, L. S., Thompson, M. Y., Di Sabatino, S. & Fernando, H. J. S. 2016 Stratified flow past a hill: dividing streamline concept revisited.*Boundary-Layer Meteorol.* **159** (3), 611–634.

Lelong, M. and T.J. Dunkerton, 1998: Inertia–Gravity Wave Breaking in Three Dimensions. Part II: Convectively Unstable Waves. J. Atmos. Sci., **55**, 2489–2501,https://doi.org/10.1175/1520-0469(1998)055<2489:IGWBIT>2.0.CO;2

Leutbecher, M., and H. Volkert, Propagation of mountain waves into the stratosphere: Quantitative evaluation of three-dimensional simulations, *J. Atmos. Sci.*, *57*, 3090–3108, 2000.

Lighthill, J. M., 1952: On sound generated aerodynamically, I. General theory, Proc. Roy. Soc. London, 211(A), 564–587.

Lilly, D.K., 1978: A Severe Downslope Windstorm and Aircraft Turbulence Event Induced by a Mountain Wave. *J. Atmos. Sci.,* **35**, 59–77, https://doi.org/10.1175/1520-0469(1978)035<0059:ASDWAA>2.0.CO;2

Lilly, D., & Klemp, J. (1979). The effects of terrain shape on nonlinear hydrostatic mountain waves. *Journal of Fluid Mechanics, 95*(2), 241-261. doi:10.1017/S0022112079001452

Lilly, D. K., and P. J. Kennedy, Observations of a stationary mountain wave and its associated momentum flux and energy dissipation, *J. Atmos. Sci.*, *30*, 1135–1152, 1973

Lin, Y.-L., R. L. Deal, and M. S. Kulie, 1998: Mechanisms of cell regeneration, development, and propagation within a two-dimensional multicell storm. J. Atmos. Sci.,**55,** 1867–1886.

Lin, Y-L., and T. A. Wang, 1996: Flow regimes and transient dynamics of two-dimensional stratified flow over an isolated mountain ridge. J. Atmos. Sci., **53,** 139–158.

Lindzen, R. S., Turbulence and stress owing to gravity wave and tidal breakdown, *J. Geophys. Res.*, *86*, 9707–9714, 1981.

Liu, H.-L. and S. L. Vadas, 2013: "Large-scale ionospheric disturbances due to the dissipation of convectively-generated gravity waves over Brazil", J. Geophys. Res, 118, 2419–2427, doi:10.1002/jgra.50244.

Lott, F. (1997), The transient emission of propagating gravity waves by a stably stratified shear layer, *Q. J. R. Meteorol. Soc.*, *123*,
1603–1619

Lott, F. (1998): Linear mountain drag and averaged pseudo-momentum flux profiles in the presence of trapped lee waves. Tellus, 50A, 12–25.

Lott, F. and Miller, M (1997): A new sub-grid orographic drag parametrization: Its formulation and testing. Q. ***J.*** *R. Meteorol. Soc.,* 123, 101-127

Lott, F., R. Plougonven, and J. Vanneste (2010), Gravity waves generated by sheared potential vorticity anomalies, *J. Atmos. Sci.*, *67*, 157–170, doi:10.1175/2009JAS3134.1.

Lott, F., R. Plougonven, and J. Vanneste (2012), Gravity waves generated by sheared three-dimensional potential vorticity anomalies, *J. Atmos. Sci.*, *69*, 2134–2151.

Lott, F., Guez, L., and Maury, P.: A stochastic parameterization of non-orographic gravity waves, Formalism and impact on the equatorial stratosphere, Geophys. Res. Lett., 39, L06807, doi:10.1029/2012GL051001, 2012.

Lott F. and L. Guez. (2013) A stochastic parameterization of the gravity waves due to convection and its impact on the equatorial stratosphere. *Journal of Geophysical Research: Atmospheres* **118**:16, 8897-8909.

Luo, Z., and D. Fritts (1993), Gravity wave excitation by geostrophic adjustment of the jet stream. Part II: Three dimensional forcing, *J.Atmos. Sci.*, *50*(1), 104–115.

Lyra, G. 1940 Über den Einfluß von Bodenerhebungen auf die Str¨omung einer stabil geschichteten Atmospha¨re. Beitr. Phys. Freien Atmos. 26, 197–206.

Lyra, G., 1943: Theorie der stationa¨ren Leewellen- str¨omung in freir Atmospha¨re, Zeit. angew. Math. Mech., 23, 1–28.

McFarlane, N.A. 1987. The effect of orographically excited gravity-wave drag on the general circulation of the lower stratosphere and troposphere. *J. Atmos. Sci.* **44**: 1775–1800.

McLandress, C., On the importance of gravity waves in the middle atmosphere and their parameterization in general circulation models, *J. Atmos. Sol. Terr. Phys.*, *60*, 1357–1383, 1998.

Medvedev, A. S., and G. P. Klaassen, Vertical evolution of gravity wave spectra and the parameterization of associated wave drag, *J. Geophys. Res.*, *100*, 25,841–25,853, 1995.

Medvedev AS, Yiğit E. Gravity Waves in Planetary Atmospheres: Their Effects and Parameterization in Global Circulation Models. *Atmosphere*. 2019; 10(9):531. https://doi.org/10.3390/atmos10090531

Miller, J. E., 1948: On the concept of frontogenesis. *J. Meteor.,* **5,** 169 –171.

Miranda, P. M. A. and James, I. N. 1992. Non-linear three-dimensional effects on gravity wave drag: splitting flow and breaking waves.Quart. J. Roy. Meteorol. Soc. 118, 1057-1081

Miyoshi, Y., H. Fujiwara, H. Jin, and H. Shinagawa (2014), A global view of gravity waves in the thermosphere simulated by a general circulation model, *J. Geophys. Res. Space Physics*, 119, 5807–5820, doi: 10.1002/2014JA019848.

McFarlane, N. A., 1987: The effect of orographically excited wave drag on the general circulation of the lower stratosphere and troposphere. J. Atmos. Sci., 44, 1775–1800.

McLandress, C., T.G. Shepherd, S. Polavarapu, and S.R. Beagley, 2012: Is Missing Orographic Gravity Wave Drag near 60°S the Cause of the Stratospheric Zonal Wind Biases in Chemistry–Climate Models?. J. Atmos. Sci., **69**, 802–818, https://doi.org/10.1175/JAS-D-11-0159.1

Mixa, T., Dörnbrack, A., & Rapp, M. (2021). Nonlinear Simulations of Gravity Wave Tunneling and Breaking over Auckland Island, *Journal of the Atmospheric Sciences*, *78*(5), 1567-1582. Retrieved Sep 30, 2021, from https://journals.ametsoc.org/view/journals/atsc/78/5/JAS-D-20-0230.1.xml

Okamoto, K., K. Sato, and H. Akiyoshi (2011), A study on the formation and trend of the Brewer-Dobson circulation, *J. Geophys. Res.,* 116, D10117, doi:10.1029/2010JD014953.

Ólafsson, H. and P. Bougeault, 1996: Nonlinear flow past an elliptic mountain ridge, J. Atmos. Sci., 53, 2465-2489

Palmer, T. N., G. J. Shutts, and R. Swinbank, Alleviation of a systematic westerly bias in general circulation and numerical weather prediction models through an orographic gravity wave drag parameterization, Q. J. R. Meteorol. Soc., 112, 1001–1039, 1986.

Pandya, R. E., and D. R. Durran, 1996: The influence of convectively generated thermal forcing on the mesoscale circulation around squall lines. J. Atmos. Sci., 53, 2924–2951, doi:10.1175/1520-0469(1996)053,2924:TIOCGT.2.0.CO;2.

Pandya, R. and Alexander, M.J. 1999.: Linear stratospheric gravity waves above convective thermal Forcing, J.Atmos.Sci., 56, 2434–2446,1999.

Pautet, P.-D., M. J. Taylor, D. C. Fritts, K. Bossert, B. P. Williams, D. Broutman, J. Ma, S. D. Eckermann, and J. D. Doyle (2016), Large-amplitude mesospheric response to an orographic wave generated over the Southern Ocean Auckland Islands (50.7°S) during the DEEPWAVE project, *J. Geophys. Res. Atmos.*, 121, 1431–1441, doi:10.1002/2015JD024336.

Peltier, W.R. and T.L. Clark, 1979: The Evolution and Stability of Finite-Amplitude Mountain Waves. Part II: Surface Wave Drag and Severe Downslope Windstorms. J. Atmos. Sci., 36, 1498–1529, https://doi.org/10.1175/1520-0469(1979)036<1498:TEASOF>2.0.CO;2

Pfister, L.; S. Scott and M. Loewenstein. 1993. Mesoscale disturbances in the tropical stratosphere excited by convection: Observations and effects on the stratospheric momentum budget. *J. Atmos. Sci*. **50**: 1058–1075.

Phillips, D. S., 1984: Analytical surface pressure and drag for linear hydrostatic flow over three-dimensional elliptical mountains. J. Atmos. Sci., 41, 1073–1084, https://doi.org/ 10.1175/1520-0469(1984)041,1073:ASPADF.2.0.CO;2.

Piani, C., D. Durran, M. Alexander, and J. Holton, 2000: A numerical study of three-dimensional gravity waves triggered by deep tropical convection and their role in the dynamics of the QBO. J. Atmos. Sci., 57, 3689–3702, doi:10.1175/1520-0469(2000)057,3689: ANSOTD.2.0.CO;2.

Piani, C., and D. Durran, 2001: A numerical study of stratospheric gravity waves triggered by squall lines observed during the TOGA COARE and COPT-81 experiments. J. Atmos. Sci.,58, 3702–3723.

Pierrehumbert, R. T., and B. Wyman, 1985: Upstream effects of mesoscale mountains. J. Atmos. Sci., 42, 977–1003.

Plougonven, R., A. Hertzog, and M. J. Alexander, 2015: Case studies of nonorographic gravity waves over the Southern Ocean emphasize the role of moisture. J. Geophys. Res. Atmos., 120, 1278–1299, doi:10.1002/2014JD022332.

Plougonven, R., Zeitlin, V., 2002: Internal gravity wave emission from a pancake vortex: an example of wave-vortex interaction in strongly stratified flows. Phys. of Fluids 14(3), 1259–1268.

Portele, T.C., A. Dörnbrack, J.S. Wagner, S. Gisinger, B. Ehard, P. Pautet, and M. Rapp, 2018: Mountain-Wave Propagation under Transient Tropospheric Forcing: A DEEPWAVE Case Study. *Mon. Wea. Rev.,* **146**, 1861–1888, https://doi.org/10.1175/MWR-D-17-0080.1

Powers, J., and R. Reed (1993), Numerical simulation of the large-amplitude mesoscale gravity wave event of 15 December 1987 in the Central United States, *Mon. Weather Rev.*, *121*, 2285–2308.

Plougonven, R., H. Teitelbaum, and V. Zeitlin (2003), Inertia-gravity wave generation by the tropospheric mid-latitude jet as given by the FASTEX radiosoundings, *J. Geophys. Res.*, *108*(D21), 4686, doi:10.1029/2003JD003535.

Plougonven, R., and F. Zhang, 2014: Internal gravity waves from atmospheric jets and fronts. Rev. Geophys., 52, doi:10.1002/2012RG000419.

Powers, J. (1997), Numerical model simulation of a mesoscale gravity-wave event: Sensitivity tests and spectral analyses, *Mon. Weather Rev.*, *125*, 1838–1869.

Queney, P. (1947), Theory of perturbations in stratified currents with applications to airflow over mountain barriers. Dept. of Meteorology. Univ. of Chicago, Misc. Report No. 23

Ray, E. A., M. J. Alexander, and J. R. Holton (1998), An analysis of structure and forcing of the equatorial semiannual oscillation in zonal wind, J. Geophys. Res., 103(D2), 1759–1774.

Richter, J., and R. R. Garcia (2006), On the forcing of the mesospheric semi-annual oscillation in the Whole Atmosphere Community Climate Model, *Geophys. Res. Lett.*, 33, L01806, doi:10.1029/2005GL024378.

Richter, J. H., Sassi, F. and Garcia, R. R. (2010) Towards a physically based gravity wave source parameterization in a general circulation model. *J. Atmos. Sci.*, **67**, 136–156.

Richter, J. H., A. Solomon, and J. T. Bacmeister (2014), On the simulation of the quasi-biennial oscillation in the Community Atmosphere Model, version 5, J. Geophys. Res. Atmos., 119, 3045–3062, doi:10.1002/2013JD021122.

Rind, D., R. Suozzo, N. K. Balachandran, A. Lacis, and G. Russell, 1988: The GISS global climate-middle atmosphere model. Part I: Model structure and climatology. *J. Atmos. Sci.,* **45,** 329–370.

Rosenlof, K. (1996), Summer hemisphere differences in temperature and transport in the lower stratosphere, J. Geophys. Res., 101, 19,129–19,136.

Ruppert, J. H., Jr., Koch, S. E., Chen, X., Du, Y., Seimon, A., Sun, Y. Q., Wei, J., and Bosart, L. F., 2021: Mesoscale Gravity Waves and Midlatitude Weather: A tribute to Fuqing Zhang, Bulletin of the American Meteorological Society (published online ahead of print 2021). from https://journals.ametsoc.org/view/journals/bams/aop/BAMS-D-20-0005.1/BAMS-D-20-0005.1.xml

Sandu, I., van Niekerk, A., Shepherd, T.G. *et al.* Impacts of orography on large-scale atmospheric circulation. *npj Clim Atmos Sci* **2,** 10 (2019). https://doi.org/10.1038/s41612-019-0065-9

Sato, K. (1994), A statistical study of the structure, saturation and sources of inertio-gravity waves in the lower stratosphere observed with the MU radar, *J. Atmos. Terr. Phys.*, *56*(6), 755–774.

Sato, K., Tateno, S., Watanabe, S., & Kawatani, Y. (2012). Gravity Wave Characteristics in the Southern Hemisphere Revealed by a High-Resolution Middle-Atmosphere General Circulation Model, *Journal of the Atmospheric Sciences*, *69*(4), 1378-1396. Retrieved Sep 30, 2021, from https://journals.ametsoc.org/view/journals/atsc/69/4/jas-d-11-0101.1.xml

Satomura, T. and K. Sato, 1999: Secondary Generation of Gravity Waves Associated with the Breaking of Mountain Waves.J. Atmos. Sci.,56,3847–3858, https://doi.org/10.1175/1520-0469(1999)056<3847:SGOGWA>2.0.CO;2

Schirber, S., E. Manzini, and M. J. Alexander (2014), A convection-based gravity wave parameterization in a general circulation model: Implementation and improvements on the QBO, J. Adv. Model. Earth Syst., 6, 264–279, doi:10.1002/2013MS000286.

Schmidt, J., and W. Cotton (1990), Interactions between upper and lower tropospheric gravity waves on squall line structure and maintenance, *J. Atmos. Sci.*, *47*, 1205–1222.

Scinocca, J., and R. Ford (2000), The nonlinear forcing of large-scale internal gravity waves by stratified shear instability, *J. Atmos. Sci.*, *57*, 653–672.

Shige, S. and T. Satomura (2000), The Gravity Wave Response in the Troposphere around Deep Convection, *J. Met. Japan, 78(6*), 789-801. https://doi.org/10.2151/jmsj1965.78.6_789

Schecter, D., 2008: The spontaneous imbalance of an atmospheric vortex at high Rossby number. J. Atmos. Sci. 65, 2498– 2521.

J. F. Scinocca and N. A. McFarlane. (2000) The parametrization of drag induced by stratified flow over anisotropic orography. Quarterly Journal of the Royal Meteorological Society **126**:568, 2353-2393.

Scinocca, J. F., McFarlane, N. A. Lazare, M., Li, J., and Plummer, D.: Technical Note: The CCCma third generation AGCM and its extension into the middle atmosphere, Atmos. Chem. Phys., 8, 7055–7074, doi:10.5194/acp-8-7055-2008, 2008.

Scorer, R. S., 1949: Theory of waves in the lee of mountains. Q. Jour. Royal Met. Soc., 75, 41-56

Serva F., C. Cagnazzo, A. Riccio and E. Manzini, Impact of a Stochastic Nonorographic Gravity Wave Parameterization on the Stratospheric Dynamics of a General Circulation Model, *Journal of Advances in Modeling Earth Systems*, 10, 9, (2147-2162), (2018).

Sheppard P. A. (1956) Airflow over mountains. Q J R Meteorol Soc, 82, 528–529

Smith R. B,., 1979: The influence of mountains on the atmosphere. Advances in Geophysics, B. Saltzman, Ed., Vol. 21, Academic Press, 87–230, https://doi.org/10.1016/S0065-2687(08)60262-9

Smith, R. B., 1980: Linear theory of stratified hydrostatic flow past an isolated mountain. *Tellus,* **32,** 348–364.

Smith, R.B., 1985: On Severe Downslope Winds. *J. Atmos. Sci.,* **42**, 2597–2603, https://doi.org/10.1175/1520-0469(1985)042<2597:OSDW>2.0.CO;2

Smith, R. B., 1989: Hydrostatic airflow over mountains. Adv. Geophys., 31, 1- 41

Smith, A. K., and G. P. Brasseur (1991), Numerical simulation of the seasonal variation of mesospheric water vapor, J. Geophys. Res., 96, 7553–7563, doi:10.1029/91JD00226.

Smith R. B., and C. G. Kruse, 2017: Broad-spectrum mountain waves.J. Atmos. Sci., 74, 1381–1402, https://doi.org/10.1175/JAS-D- 16-0297.1.

Smolarkiewicz, P. K., and R. Rotunno, 1990: Low Froude number flow past three-dimensional obstacles. Part II: Upwind flow reversal zone. J. Atmos. Sci., 47, 1498–1511.

Smith, R.B., A.D. Nugent, C.G. Kruse, D.C. Fritts, J.D. Doyle, S.D. Eckermann, M.J. Taylor, A. Dörnbrack, M. Uddstrom, W. Cooper, P. Romashkin, J. Jensen, and S. Beaton, 2016: Stratospheric Gravity Wave Fluxes and Scales during DEEPWAVE. *J. Atmos. Sci.,* **73**, 2851–2869, https://doi.org/10.1175/JAS-D-15-0324.1

Smith, R.B. and C.G. Kruse, 2017: Broad-Spectrum Mountain Waves. *J. Atmos. Sci.,* **74**, 1381–1402, https://doi.org/10.1175/JAS-D-16-0297.1

Smith, R.B. and C.G. Kruse, 2018: A Gravity Wave Drag Matrix for Complex Terrain. *J. Atmos. Sci.,* **75**, 2599–2613, https://doi.org/10.1175/JAS-D-17-0380.1

Smith, R. B., 2019: 100 years of progress on mountain meteorology research. Book chapter under review.

Snively, J. B., and V. P. Pasko (2008), Excitation of ducted gravity waves in the lower thermosphere by tropospheric sources, *J. Geophys. Res.*, *113*, A06303, doi:10.1029/2007JA012693.

Song, I.-S., H.-Y. Chun, and T. P. Lane, 2003: Generation mechanisms of convectively forced internal gravity waves and their propagation to the stratosphere. *J. Atmos. Sci.*, **60**, 1960–1980, doi:https://doi.org/10.1175/1520-0469(2003)060<1960:GMOCFI>2.0.CO;2.

Song I-S. and H-Y. Chun (2005) Momentum Flux Spectrum of Convectively Forced Internal Gravity Waves and Its Application to Gravity Wave Drag Parameterization. Part I: Theory. *Journal of the Atmospheric Sciences* **62**:1, 107-124.

Song, I.-S., and H.-Y. Chun 2008: A Lagrangian spectral parameterization of gravity wave drag induced by cumulus convection. J. Atmos. Sci., 65, 1204–1224.

Stephan, C., M.J. Alexander, and J.H. Richter, 2016: Characteristics of Gravity Waves from Convection and Implications for Their Parameterization in Global Circulation Models. J. Atmos. Sci., **73**, 2729–2742, https://doi.org/10.1175/JAS-D-15-0303.1

Su, T., & Zhai, G. (2017). The role of convectively generated gravity waves on convective initiation: A case study. *Monthly Weather Review*,*145*, 335–359.

Sugimoto, N., Ishioka, K., Ishii, K., 2008: Parameter sweep experiments on spontaneous gravity wave radiation from unsteady rotational flow in an f-plane shallow water system. J. Atmos. Sci. 65, 235–249.

Tabaei, A., and T. R. Akylas, 2007: Resonant long-short wave interactions in an unbounded rotating stratified fluid. Stud. Appl. Math., 119, 271–296.Uccellini, L., and S. Koch (1987), The synoptic setting and possible energy sources for mesoscale wave disturbances, *Mon. Weather Rev.*, *115*, 721–729.

Teixiera, M. A. C., 2014: The physics of orographic gravity wave drag. Frontiers in Physics, https://doi.org/10.3389/fphy.2014.00043

Vadas, S. L., D. C. Fritts, and M. J. Alexander(2003),Mechanism for the generation of secondary waves in wave breaking regions,J. Atmos. Sci., 60, 194–214.

Vadas, S.L., J. Zhao, X. Chu and E. Becker, 2018, "The Excitation of secondary gravity waves from local body forces: Theory and observation", J. Geophys. Res. Atmospheres, 123, https://doi.org/10.1029/2017JD027970.

Vadas, S.L., H.-L. Liu, and R.S. Lieberman, 2014, "Numerical modeling of the global changes to the thermosphere and ionosphere from the dissipation of gravity waves from deep convection", JGR Space Physics, 119, doi:10.1002/2014JA020280

Vadas, S.L., J. Zhao, X. Chu and E. Becker, 2018, "The Excitation of secondary gravity waves from local body forces: Theory and observation", J. Geophys. Res. Atmospheres, 123, https://doi.org/10.1029/2017JD027970.

Vadas, S. L. and M. J. Nicolls, 2012, "The Phases and Amplitudes of Gravity Waves Propagating and Dissipating in the Thermosphere: Theory", J. Geophys. Res, 117, A05322, doi:10.1029/2011JA017426.

Vadas, S. L., and D. C. Fritts, 2005: "Thermospheric responses to gravity waves: Influences of increasing viscosity and thermal diffusivity", J. Geoph. Res.,{110, D15103}'{doi:10.1029/2004JD005574}.

Vadas, S. L. 2007: "Horizontal and vertical propagation, and dissipation of gravity waves in the thermosphere from lower atmospheric and thermospheric sources", J. Geoph. Res., {112}'{A06305, doi:10.1029/2006JA011845}.

Vadas, S. L., and M. J. Nicolls (2012), The phases and amplitudes of gravity waves propagating and dissipating in the thermosphere: Theory,J. Geophys. Res., 117, A05322, doi:10.1029/2011JA017426.

Van den Bremer, T. S., and B. R. Sutherland, 2014: The mean flow and long waves induced by two-dimensional internal gravity wavepackets. Phys. Fluids, 26 (10), 106601, doi:10.1063/1. 4899262.

Vanneste, J. (2008), Exponential smallness of inertia-gravity-wave generation at small rossby number, *J. Atmos. Sci.*, *65*, 1622–1637.

Vanneste, J., and I. Yavneh (2004), Exponentially small inertia-gravity waves and the breakdown of quasi-geostrophic balance, *J. Atmos. Sci.*, *61*, 211–223.

Vincent, R. A., S. J. Allen, and S. D. Eckermann, 1997: Gravity wave parameters in the lower stratosphere. Gravity Wave Processes: Their Parameterization in Global Climate Models,K. Hamilton, Ed., Springer, 7–25.

Wang, J., Kim, H.-M., & Chang, E. K. M. (2018). Interannual modulation of Northern Hemisphere winter storm tracks by the QBO. *Geophysical Research Letters*, *45*. https://doi.org/10.1002/ 2017GL076929

Walterscheid, R. L., and M. P. Hickey (2011), Group velocity and energy flux in the thermosphere: Limits on the validity of group velocity in a viscous atmosphere, *J. Geophys. Res.*, 116, D12101, doi: 10.1029/2010JD014987.

Wang, J., H.-M. Kim, E. K. M. Chang, and S.-W. Son, 2018: Modulation of the MJO and North Pacific storm track relationship by the QBO. J. Geophys. Res. Atmos., 123, 3976– 3992, https://doi.org/10.1029/2017JD027977.

Wang, L., and M. Geller (2003), Morphology of gravity-wave energy as observed from 4 years (1998–2001) of high vertical resolution U.S. radiosonde data, *J. Geophys. Res.*, *108*, 4489, doi:10.1029/2002JD002786.

Warner, C. D., and M. E. McIntyre, An ultra-simple spectral parameterization for non-orographic gravity waves, *J. Atmos. Sci.*, *58*, 1837–1857, 2001

Webster, S., A. R. Brown, D. R. Cameron, and C. P. Jones, 2003: Improvements to the representation of orography in the Met Office Unified Model. Quart. J. Roy. Meteor. Soc., 129, 1989– 2010, https://doi.org/10.1256/qj.02.133.

Wei, J., and F. Zhang, 2014: Mesoscale gravity waves in moist baroclinic jet–front systems. J. Atmos. Sci., 71, 929–952, doi:10.1175/JAS-D-13-0171.1.

Wei, J., and F. Zhang, 2015: Tracking gravity waves in moist baroclinic jet-front systems. J. Adv. Model. Earth Syst., 7, 67-91, doi: 10.1002/2014MS000395

Wei, J., F. Zhang, and J. H. Richter, 2016: An analysis of gravity wave spectral characteristics in moist baroclinic jet-front systems. J. Atmos. Sci., 73, 3133–3155, doi:10.1175/JAS-D-15-0316.1.

Wei, J., G. Bölöni, and U. Achatz, 2019: Efficient modelling of the interaction of mesoscale gravity waves with unbalanced large-scale flows: Pseudomomentum-flux convergence versus direct approach. J. Atmos. Sci., 76, 2715-2738, doi: https://doi.org/10.1175/JAS-D-18-0337.1

Wilhelm, J., T. R. Akylas, G. Bölöni, J. Wei, B. Ribstein, R. Klein, and U. Achatz, 2017: Interactions between Mesoscale and Submesoscale Gravity Waves and Their Efficient Representation in Mesoscale-Resolving Models. J. Atmos. Sci., 75, 2257-2280, doi: https://doi.org/10.1175/JAS-D-17-0289.1

Winters, K., & Armi, L. (2014). Topographic control of stratified flows: Upstream jets, blocking and isolating layers. *Journal of Fluid Mechanics, 753*, 80-103. doi:10.1017/jfm.2014.363

Wu, D. L., and F. Zhang, 2004: A study of mesoscale gravity waves over the North Atlantic with satellite observations and a mesoscale model. J. Geophys. Res., 109, D22104, doi:10.1029/ 2004JD005090.

Yiğit, E., A. S. Medvedev, A. D. Aylward, P. Hartogh, and M. J. Harris (2009), Modeling the effects of gravity wave momentum deposition on the general circulation above the turbopause, *J. Geophys. Res.*, 114, D07101, doi: 10.1029/2008JD011132.

Yiğit, E., and A. S. Medvedev (2009), Heating and cooling of the thermosphere by internal gravity waves, *Geophys. Res. Lett.*, 36, L14807, doi: 10.1029/2009GL038507.

Yoo, C., and S.-W. Son (2016), Modulation of the boreal wintertime Madden-Julian oscillation by the stratospheric quasi-biennial oscillation,Geophys. Res. Lett., 43, 1392–1398, doi:10.1002/2016GL067762.

Yu, Y., W. Wang and M. P. Hickey (2017), Ionospheric signatures of gravity waves produced by the 2004 Sumatra and 2011 Tohoku tsunamis: A modeling study, *J. Geophys. Res. Space Physics*, 121, doi:10.1002/2016JA023116.

Su T. and Guoqing Zhai. (2017) The Role of Convectively Generated Gravity Waves on Convective Initiation: A Case Study. Monthly Weather Review **145**:1, 335-359.

Zhang, F., 2004: Generation of mesoscale gravity waves in the upper- tropospheric jet-front systems. J. Atmos. Sci., 61, 440–457.

Zhang, D.-L., and J. Fritsch (1988), Numerical simulation of the meso-b scale structure and evolution of the 1977 Johnstown flood. Part III: Internal gravity waves and the squall line, *J. Atmos. Sci.*, *45*, 1252–1268.

Zhang, F., and S. Koch (2000), Numerical simulations of a gravity wave event over CCOPE. Part II: Waves generated by an orographic density current, *Mon. Weather Rev.*, *128*(8), 2777–2796.

Zhang, F., S. Koch, C. Davis, and M. Kaplan (2001), Wavelet analysis and the governing dynamics of a large amplitude mesoscale gravity wave event along the east coast of the united states, *Q. J. R. Meteorol. Soc.*, *127*, 2209–2245.

Zhang, F., S. Koch, and M. Kaplan (2003), Numerical simulations of a large-amplitude gravity wave event, *Meteo. Atmos. Phys.*, *84*, 199–216.

Zhang, S., and F. Yi (2005), A statistical study of gravity waves from radiosonde observations at Wuhan (30 degrees N, 114 degrees E) China, *Ann. Geophys.*, *23*, 665–673.

Zhang, S., and F. Yi (2008), Intensive radiosonde observations of gravity waves in the lower atmosphere over Yichang (111 degrees 18’ E, 30 degrees 42’ N), China, *Ann. Geophys.*, *26*(7), 2005–2018.